Astron. Astrophys. 350, 204–229 (1999)

ASTRONOMY AND ASTROPHYSICS

Time dependent chemical models of spherical dark clouds

L.A.M. Nejad[1] **and R. Wagenblast**[2]

[1] Department of Computing and Mathematics, The Manchester Metropolitan University, Manchester M1 5GD, UK
[2] Physics Department, UMIST, P.O. Box 88, Manchester M60 1QD, UK

Received 21 December 1998 / Accepted 26 July 1999

Abstract. We present detailed time and depth dependent chemical models of low mass dark molecular cloud cores. The cloud is assumed to be in hydrostatic equilibrium with a density and pressure structure described by a polytropic equation of state with negative polytropic index and boundary conditions at the centre and the edge of the cloud constrained by observations of dense and diffuse clouds. We study cloud models with a diameter of ~ 1 pc, central core temperature of 10 K, core central densities in the range of $(2-10)\times10^4\,\mathrm{cm}^{-3}$, surface pressures $\frac{P}{k}$ ranging from $\sim$ 1–$3\times10^4\,\mathrm{cm}^{-3}$K and turbulent velocities of $\lesssim 0.4\,\mathrm{km\,s}^{-1}$. The cloud is assumed to be subject to cosmic-ray ionization and exposed to the interstellar UV radiation field. We assumed two different geometries for the UV radiation field; one in which the cloud is subject to an isotropic field and the other in which the cloud is exposed to a radiation field in the direction of the observer from both sides, resembling a simple 2-D chemical time and depth dependent model. For calculating the H_2 density profile and the fractions of atomic and molecular hydrogen as a function of radius we assume an equilibrium of H_2 photodissociation and H_2 formation on grains, taking into account the H_2 self-shielding and dust extinction. The models incorporate time dependent chemical evolution of abundances and column densities of 175 species containing heavy elements C, O, N, S and Na with a C/O ratio of ~ 0.55, assuming a depth dependent sulphur depletion which decreases linearly with increasing density from the edge to the centre of the cloud. Chemical models include the effects of additional photons generated by cosmic rays, CO accretion onto dust grains and desorption of CO mantles by direct cosmic-ray heating. The results show that cosmic-ray-induced internal photons, by increasing mainly the C^+ abundance, make order-of-magnitude difference in the predicted abundances of species notably those whose maximum abundances are reached during the so-called "early-times" of a few$\times10^5$ years. Closer chemical connections between HC_3N, C_2S and C_3H_2 have been found under influence of cosmic-ray-induced photo reactions. CO is the key molecule in controlling the chemistry at later times and its loss onto grains critically affects the abundances of the so-called "late type" species; when the CO abundance builds up then the dominant ion H_3^+ is used up in the production and destruction reactions sequence of CO, $\mathrm{CO}\xrightarrow{\mathrm{H_3^+}}\mathrm{HCO^+}\xrightarrow{\mathrm{e}}\mathrm{CO}$, deactivating the overall remaining chemistry. With the loss of CO from the gas phase, H_3^+ becomes available to stimulate the chemistry of non-carbon containing species, thus contributing significantly in increasing the predicted column density of NH_3 and N_2H^+ to match their observed values. With depletion of CO from the gas phase, and subsequent overall change in C:O:N:S abundance ratios, close chemical relations between abundance variations of SO and N_2H^+ with NH_3 are found. Direct desorption by cosmic-ray heating is found to be efficient in recovering the observed gas-phase CO abundance, and provide conditions under which the chemical equilibrium in the cloud is established at ~ 5 million years. The results presented include: the time variation of abundances corresponding to the centre of the cloud, variation of abundances with radius and A_v for selected evolution times along the central line of sight, time variation of the column density of selected observed species along the central line of sight and average column densities integrated over various beam sizes. The calculated average column densities for various beam sizes indicate that the models account for the observed size of the maps of HC_3N (~ 0.1 pc), NH_3 (~ 0.15 pc) and C_2S (~ 0.25 pc). Comparisons are made with observations.

Key words: ISM: clouds – ISM: structure – ISM: molecules – ISM: abundances – stars: formation

1. Introduction

Low mass cores are associated with many nearby dark clouds. They are notable for their narrow, nearly thermal line widths and their connection with low mass stars. To understand the physical and chemical conditions and to extend our knowledge of their evolutionary stages it is important to construct cloud models that use density and temperature distributions that are as close as possible to the observed physical conditions.

High spectral and spatial resolution mapping observations of molecular lines now provide a much more detailed description of the physical and chemical conditions in the cloud including temperature and density structure and spatial distribution of various molecules. Along with the progress in observations of dark clouds and improved measurements of molecular abundances,

Send offprint requests to: L.A.M. Nejad
Correspondence to: L.A.M. Nejad (L.Nejad@doc.mmu.ac.uk)

comprehensive time dependent chemical models incorporating detailed physical processes have been developed to study the dominant chemical reactions and assessing the influence of various processes on the chemistry, aiming to explain the observed molecular abundances and to understand the physical properties and overall stages of the cloud evolution. Detailed dense cloud chemical models include early steady-state models of Herbst & Klemperer (1973), Mitchell et al. (1978), Millar & Freeman (1984) and time dependent models of Iglesias (1977), Prasad & Huntress (1980), Graedel et al. (1982), Millar & Nejad (1985) and Herbst & Leung (1986). During the last decade detailed gas phase chemical models became more comprehensive by incorporating the effects of dust grain interactions and gas dynamics appropriate to star forming regions (Charnley et al. 1988; Nejad et al. 1990; Rawlings et al. 1992; Hartquist et al. 1993; Howe et al. 1996). Most of these studies have used one point models and have ignored depth dependent effects of the physical conditions and chemical abundances. Although these model assumptions appear to be adequate for explaining the observed abundances of some molecules for the conditions close to the centre of dense cloud cores, they are insufficient to show the depth dependent effects of temperature, density and ionization variations on the cloud chemistry. It is particularly important to include the depth dependent effects in the study of dark molecular clouds, which have been observed to have clumpy structure, containing a dense core component surrounded by a low density cloud and subject to radiation effects from internal sources as well as the effects from nearby star formation. Furthermore, observations of dark molecular cores are used to derive total column densities of chemical species, i.e. the numbers of molecules within the column traced by the telescope beam. Consequently, depth dependent models which predict column densities are much better suited for the interpretation of observational data than one point models which only can produce the relative abundance of chemical species for a single point in the cloud.

The importance of models in which density and temperature vary with depth into the cloud was suggested by Black & Dalgarno (1977) and several models have been constructed; Boland & de Jong (1984) have studied detailed hydrostatic spherical models of dense clouds assuming thermal balance and steady-state chemistry. In diffuse clouds, van Dishoeck & Black (1986) studied comprehensive depth dependent spherical models, assuming a polytropic equation of state, with a detailed treatment of the radiative transfer, and a steady-state chemistry. Sternberg & Dalgarno (1995) used depth dependent models to study the chemical structure of dense photon-dominated regions (PDRs) assuming steady-state conditions. Xie et al. (1995) have used time dependent 1-D models with variable density to study the effects of turbulent diffusion in the gas-phase chemistry of small molecules. Lee et al. (1996) have constructed time dependent chemical models of quiescent dense clouds to study the photodissociation of H_2 and CO in the context of an inhomogeneous cloud model divided into 43 slabs, assuming a constant temperature and a density variation by two orders of magnitude from the surface to the centre of the cloud. More recently, Turner et al. (1998) have studied the time dependent chemistry of small translucent clouds using models with total extinction (i.e. twice the $A_{\rm v}$ at the centre of the cloud) varying from 0.25–5 mag in steps of 0.25 mag, and one model with a total $A_{\rm v}$ of 10 mag representative of dense cloud conditions, assuming a constant density and a temperature variation as a function of $A_{\rm v}$. In summary, these depth dependent studies either considered steady-state chemistry with spherical geometry or time dependent chemistry and plane parallel geometry. For denser clouds it is known that the abundances of several key trace molecules strongly vary with time. As it was noted by de Jong et al. (1980) and Boland & de Jong (1984), the plane parallel models appear to be very centrally condensed and thus suitable for modelling small molecular cloud cores. Therefore for more extended clouds, which show a core-envelope structure, spherical cloud models are probably more realistic than plane parallel ones in predicting column densities. Our principal aim in this study has been to develop time dependent models with spherical geometry to study both depth and time dependent effects of the chemical evolution and physical processes pertained in low mass dense cloud cores. In this paper we are presenting the basic model and some preliminary results. However, the computational formulation which we have developed for this work can be applied for detailed studies of molecular clouds which are not in hydrostatic equilibrium.

The polytropic model assumptions have been adopted for the conditions of interstellar clouds (Viala 1972a, b; Shu et al. 1972) and it has been shown that polytropes with index $\Gamma < -1$ can provide a reasonable approximation for the density and temperature profiles within these clouds. In this paper we present polytropic spherical models of low mass molecular clouds assuming no internal source of radiation, using a detailed time dependent chemistry including the effects of UV photodissociation, cosmic-ray ionization, cosmic-ray-induced (CRI) photoionization and photodissociation reactions, CO depletion onto grains and desorption by cosmic-ray spot heating of the CO mantles.

The plan of this paper is as follows. In Sect. 2 we describe the polytropic model in detail, consider physical parameters and discuss relevant observations. The results for the polytropic structure of the cloud are presented at the end of Sect. 2. Details of the chemical models and the important aspects of the chemical assumptions and formulations that we have adopted are discussed in Sect. 3. Results, including chemical analyses of several species, are presented and discussed in Sect. 4, followed by concluding remarks in Sect. 5.

2. Polytropic cloud structure

2.1. Basic equations

To describe the internal structure of the cloud we assume a static spherical model with the polytropic equation of state,

$$P = K\rho^{\frac{\Gamma+1}{\Gamma}} \tag{1}$$

where P is the gas pressure, K is the polytropic constant and Γ is the polytropic index which is a free parameter. Detailed

physical interstellar cloud models assuming local thermal balance (Viala 1972a, b; Shu et al. 1972) indicate that polytropes with negative index $\Gamma < -1$ provide a reasonable approximation of the cloud structure; for a full discussion of the properties of negative indexed polytropes see Viala & Horedt (1974) and Maloney (1988). In addition, the pressure P and mass density ρ must satisfy the equation of hydrostatic equilibrium,

$$\frac{\mathrm{d}P}{\mathrm{d}r} = -\frac{Gm\rho}{r^2} \tag{2}$$

and the conservation of mass m,

$$\frac{\mathrm{d}m}{\mathrm{d}r} = 4\pi r^2 \rho \tag{3}$$

where r is the cloud radius and G is the gravitational constant.

Using normalized variables, $\tilde{P} = \frac{P}{P_\mathrm{e}}$, $\tilde{\rho} = \frac{\rho}{\rho_\mathrm{e}}$ and $\tilde{r} = \frac{r}{r_\mathrm{e}}$, where subscript e denotes the value of the variable at the edge of the cloud, eliminating mass m, we derive a second order differential equation in $\tilde{\rho}$ with respect to normalized cloud radius $\tilde{r}$,

$$\frac{\mathrm{d}^2\tilde{\rho}}{\mathrm{d}\tilde{r}^{\,2}} = -\frac{1}{\tilde{r}\tilde{\rho}^{\frac{1-2\Gamma}{\Gamma}}}\left[2\tilde{\rho}^{\frac{1-2\Gamma}{\Gamma}}\frac{\mathrm{d}\tilde{\rho}}{\mathrm{d}\tilde{r}} + \tilde{r}\left(\frac{1-\Gamma}{\Gamma}\right)\tilde{\rho}^{\frac{1-3\Gamma}{\Gamma}}\left(\frac{\mathrm{d}\tilde{\rho}}{\mathrm{d}\tilde{r}}\right)^2 - \frac{\tilde{r}}{C}\right] \tag{4}$$

where C is a constant depending on the initial conditions at the cloud surface. The initial values of density ρ and cloud size r can be chosen arbitrarily. The solution of the initial-value problem (4) for a set of initial conditions gives the corresponding normalized density profile along the central line of sight.

To derive a temperature profile, we assume that both thermal and turbulent motions contribute to the internal pressure of the cloud,

$$\frac{P}{k} = \sum_i n_i T + \frac{(\Delta v)^2 \rho}{2k} \quad \mathrm{cm^{-3}K} \tag{5}$$

(van Dishoeck & Black 1986), where k is Boltzmann's constant, $\Delta v = 10^5 b$ is the Gaussian velocity dispersion which characterises the turbulence broadening Δv in $\mathrm{cm\,s^{-1}}$ and b in $\mathrm{km\,s^{-1}}$. In Eq. (5) the summation is over the constituents of the gas, mainly H, H_2 and He with densities n_i (in particles per $\mathrm{cm^3}$). Assuming a total hydrogen number density $n_\mathrm{H} \equiv n(\mathrm{H}) + 2n(\mathrm{H_2})$, and $n(\mathrm{He}) = 0.075\, n_\mathrm{H}$, a temperature profile can be found from,

$$T = \left[\frac{P}{n_\mathrm{H}\, k} - 78.7\, b^2\right] \,/\, (1.075\text{–}0.5\, f) \tag{6}$$

where $f = \frac{2n(\mathrm{H_2})}{n_\mathrm{H}}$ (van Dishoeck & Black 1986). In order to derive the H_2 density profile, $n(\mathrm{H_2}|r)$, we assume an equilibrium of H_2 photodissociation with a photodissociation rate $\gamma_{\mathrm{H_2}}$ and H_2 grain formation,

$$\gamma_{\mathrm{H_2}}(N_\mathrm{H}, N(\mathrm{H_2}), b)\; n(\mathrm{H_2}) = \Gamma_{gr}\; n_\mathrm{H}\; n(\mathrm{H}) \tag{7}$$

with grain formation rate coefficient $\Gamma_{gr} = 3 \times 10^{-17}$ $\mathrm{cm^3 s^{-1}}$, N_H the total hydrogen number column density and N(H_2) the column density of H_2 molecules. The unshielded H_2 photodissociation rate $\gamma_{\mathrm{H_2}}(N_\mathrm{H} = 0)$ is proportional to the strength of the interstellar UV radiation field; we used the standard UV field of Draine (1978). We adopted a value of $3 \times 10^{-11}\ \mathrm{s^{-1}}$ for the unshielded H_2 photodissociation rate at the cloud surface using calculations of Wagenblast & Hartquist (1988) without taking account of the accurate dependence of the H_2 photodissociation rate on the rotational excitation state of H_2, i.e. assuming all H_2 is in the $J = 0$ state. Inside the cloud the H_2 photodissociation rate is reduced by the effects of H_2 self-shielding and grain extinction of the external UV photon flux; H_2 self-shielding was treated according to Federman et al. (1979) and the effects of the grain extinction as described by Wagenblast & Hartquist (1989) using a grain albedo $\omega = 0.3$ and a mean scattering angle cosine $g = 0.8$ as suggested by Chlewicki & Greenberg (1984). The equilibrium H_2 density distribution, $n(\mathrm{H_2}|r)$, can be calculated as an iterative solution of Eq. (7), working from the cloud surface towards the centre in order to get consistent results with respect to H_2 self-shielding. The density profile, $n(\mathrm{H_2}|r)$, derived here is used as initial value for the chemical cloud models.

Once $n(\mathrm{H_2}|r)$ is calculated, the temperature variation, $T(r)$, within the cloud can be obtained by Eq. (6) using the density profile, $n_\mathrm{H}(r)$, and the polytropic equation of state (1) for the gas pressure, $P(r)$, inside the cloud; the turbulent pressure contribution to $P(r)$ is assumed to be constant throughout the cloud and proportional to b^2.

The visual extinction, $A_\mathrm{v}(r)$, at a point with distance r from the centre of the cloud is proportional to the corresponding total hydrogen number column density, $N_\mathrm{H}(r)$, and is calculated according to relation (Bohlin et al. 1978),

$$A_\mathrm{v}(r) = \frac{N_\mathrm{H}(r)}{1.6 \times 10^{21}\ \mathrm{cm^{-2}}} \tag{8}$$

The cloud size for a polytropic model can be determined when a given visual extinction, $(A_\mathrm{v})_\mathrm{c}$, or temperature, T_c, for the centre of the cloud is reached; here subscript c denotes the value of the parameter at the centre of the cloud.

In summary, a numerical solution of the polytropic model yields profiles of the total density $n_\mathrm{H}(r)$, the H_2 equilibrium density $n(\mathrm{H_2}|r)$, the fraction of all hydrogen which is in molecular form $f(r)$, temperature $T(r)$ and visual extinction $A_\mathrm{v}(r)$. Using these profiles, along a line of sight offset from the centre of the cloud at a distance denoted by z, at various positions x, the chemical abundances, $\alpha(x,t)|_z$, are calculated as a function of time t. The column density of species along each line of sight is calculated using the corresponding chemical abundances as a function of time. In our cloud models average column densities $\bar{N}$ are calculated, simulating observations centred at the cloud core, with a beam radius R, using the following formula,

$$\bar{N}_\alpha(R) = \frac{2\pi \int_0^R N_\alpha(z)\, z\, \mathrm{d}z}{\pi R^2} \tag{9}$$

The total column densities are integrated from the outer boundary half way through the cloud and then doubled.

2.2. Observational constraints

The variation of temperature within dense cloud cores has been studied extensively in several observational surveys using various beam sizes, different molecules and transitions. Benson & Myers (1989) using NH_3 observations of dense cores in dark clouds reported a kinetic temperature of $T_c \sim 10 \pm 2$ K for most cores. Fuller & Myers (1993) who used observations of HC_3N and NH_3 and measured velocity dispersions, derived a mean kinetic temperature of $T_c = 9.2 \pm 0.2$ K and they found this to be in good agreement with the value of $T_c = 10.2 \pm 0.6$ K determined from NH_3 observations of the same objects. The kinetic temperatures reported from observations of dense cores are generally in the range 8–15 K (Wolkovitch et al. 1997). We have studied models with a temperature at the centre of the cloud in the range $T_c \sim$ 7.5–10 K, however, for our standard model we use $T_c = 10$ K.

For regions with an intermediate gas density of about $6 \times 10^3\,\mathrm{cm}^{-3}$, a kinetic temperature of 15 K has been derived by Langer et al. (1995) from the $C^{18}O$ observations. Using the data for low mass clumps observed in Taurus Molecular Cloud-1 (TMC-1), Peng et al. (1998) suggested that the inter-clump gas (density $\sim 2 \times 10^3\ \mathrm{cm}^{-3}$) would need to have a temperature of ~ 40 K to confine the clumps under thermal pressure. For the outer boundary of the cloud with densities of a few$\times 10^2\ \mathrm{cm}^{-3}$, we adopted for various models a surface temperature in the range of $T_e \sim$ 50–70 K in agreement with diffuse cloud studies (e.g. Lambert et al. 1994).

For small regions of about 0.02–0.03 pc the carbon chain molecule C_2S is known to be an excellent tracer for investigating density, temperature, and velocity structure of dense cores and it has been used widely in observations (Suzuki et al. 1992; Langer et al. 1995; Wolkovitch et al. 1997; Peng et al. 1998). From C_2S observations, assuming kinetic temperatures in the range of 8–10 K, an H_2 density of $\sim$few$\times 10^4\ \mathrm{cm}^{-3}$ has been measured by Wolkovitch et al. (1997), which is on the lower limit of the range of $(4\text{–}40) \times 10^4\ \mathrm{cm}^{-3}$ reported by Hirahara et al. (1992) using $C^{34}S$ observations. Similarly, using C_2S lines, Suzuki et al. (1992) derived an H_2 density in the range of $(0.5\text{–}5)\times 10^4\ \mathrm{cm}^{-3}$ for dense cloud cores assuming a gas kinetic temperature of 10 K. We have considered H_2 densities in the range $(2\text{–}10)\times 10^4\ \mathrm{cm}^{-3}$.

In this study we have adopted a constant nonthermal velocity dispersion b (in km s^{-1}). We examined the effects of varying b on the temperature distribution in several models. A core kinetic temperature of $T_c = 10$ K constrains the choice of b values. Depending on the assumed H_2 density in the centre of the cloud, we examined models with a maximum b value of about 0.4 km s^{-1}. This is an upper limit derived from observations of dense cores without stars. In a study of 12 low mass cores without stars Benson (1986) found an average NH_3 line width of 0.27 ± 0.06 km s^{-1}. Myers (1990), using NH_3 observation of dense cores, reported values of b in the range of 0.2–0.4 km s^{-1}. Fuller & Myers (1993) derived smaller values in the range of 0.082–0.194 km s^{-1} from NH_3 observations and a range of 0.058–0.15 km s^{-1} from HC_3N line observations. Langer et al. (1995) observed cores located in TMC-1 and reported line widths in the range of 0.15–0.17 km s^{-1} from C_2S lines and a range of 0.11–0.15 km s^{-1} using HC_7N lines.

In our spherical cloud models the assumption that the thermal component of the line broadening, Δv_T, dominates the nonthermal component, Δv_{NT} is consistent with observations of dark cloud cores. For quiescent low mass dense cores Langer et al. (1995) reported $\Delta v_{NT} < \Delta v_T$ indicating that the gas is mainly supported by thermal pressure.

Although the nonthermal contribution is observed to be as small as 0.004 km s^{-1} in some low mass cores, there is strong observational evidence for the presence of a nonthermal line component at even the smallest observed radii in these cores (Fuller & Myers 1992). For low mass cores the ratio of nonthermal to thermal velocity dispersion for a molecule of mean molecular weight 2.3 amu, allowing for 10% helium, is given to be about 0.3–0.5 (Myers 1990). In our models this ratio typically varies between 0.3–0.8 depending on the choice of parameter values and it increases towards the centre of the cloud for higher densities.

Detailed molecular line observations of low mass cores in dense clouds, using the trace molecules CO, CS, NH_3 and HC_3N generally agree in that the cores extend to about 0.27 pc for CS and 0.15 pc for NH_3 lines (Myers et al. 1991; Langer et al. 1995). For our polytropic models we examined clouds with radii of about 0.5–0.8 pc. Within this range we found that the cloud core radii are about 0.2–0.3 pc (e.g. from the radial distribution of predicted abundances) surrounded by a more extended less dense envelope, and that the core radii did not vary greatly with the adopted cloud radius range. Therefore, we assumed a spherical cloud with a radius of $r_e \sim 0.6$ pc for all models presented here.

2.3. Polytropic model results

Table 1 lists typical models with the associated boundary conditions and the free parameters, the polytropic index Γ and the turbulent velocity b (in km s^{-1}). Note that for models 1(a,b), 2(a,b) and 3(a,b) we have chosen an $(A_v)_c = 8$ mag (i.e. the total extinction is $2 \times (A_v)_c = 16$ mag) and a temperature $T_c = 10$ K for the centre of the cloud. These models were chosen so that the values of b are within the observed range of values for dark clouds cores, particularly those without stars. It can be seen that the turbulent velocity decreases with increasing core density. For densities $n_H \gtrsim 6 \times 10^4\ \mathrm{cm}^{-3}$ the polytropic results indicate that the cloud is supported by thermal pressure and the non-thermal component of the pressure is negligible. The results in Table 1 indicate also that, if the density in the core is above $(n_H)_c \sim 6 \times 10^4\ \mathrm{cm}^{-3}$ and $(A_v)_c = 8$ mag at the centre of the cloud, then it is not possible to obtain core temperatures greater than $T_c \sim 8.4 \pm 0.2$ K. This implies that the lower limit core temperature of about 8 K reported from the observations of dense cloud cores, is probably associated with denser cores. In Table 1, models 5a to 5d display results for polytropic models with a density of $(n_H)_c = 10^5\ \mathrm{cm}^{-3}$. For this case, we have examined $(A_v)_c = 10$ and 12 mag;

Table 1. Physical parameter of polytropic models for dark clouds with a radius $r_{\rm e} = 2 \times 10^{18}$ cm. Note that at the edge of the cloud a total hydrogen density $(n_{\rm H})_{\rm e} = 200$–$400\,{\rm cm}^{-3}$ was assumed in order to satisfy boundary conditions.

Model	Γ	$(n_{\rm H})_{\rm c}$ $[{\rm cm}^{-3}]$	$T_{\rm e}$ [K]	$T_{\rm c}$ [K]	$(A_{\rm v})_{\rm c}$ [mags]	b $[{\rm km\,s}^{-1}]$
1a	−4.6	2×10^4	50	10	8	0.40
1b	−3.5	2×10^4	70	10	8	0.41
2a	−3.3	3×10^4	50	10	8	0.26
2b	−2.7	3×10^4	70	10	8	0.27
3a	−2.6	5×10^4	50	10	8	0.05
3b	−2.2	5×10^4	70	10	8	0.06
4a	−2.4	6×10^4	50	8.3	8	<0.001
4b	−2.1	6×10^4	70	8.4	8	<0.001
5a	−2.5	1×10^5	50	7.3	10	<0.001
5b	−2.0	1×10^5	70	7.5	10	<0.001
5c	−3.0	1×10^5	50	10	12	0.084
5d	−3.0	1×10^5	50	8	12	0.15

with a core $(A_{\rm v})_{\rm c} = 10$ mag a maximum core temperature of about 7.5 K was obtained. However, with a core extinction of 12 mag, core temperatures of 8 K and 10 K were obtained depending on the value chosen for the turbulent velocity b. These cloud models, models 5c and 5d, suggest that depending on the cloud conditions, nonthermal kinetic energy could be present in very dense cores. As is illustrated in Table 1, the variation in b values, for a given core density $(n_{\rm H})_{\rm c}$, is negligible for cloud surface temperatures of $T_{\rm e} \sim$ 50–70 K and surface densities of $(n_{\rm H})_{\rm e} \sim 200$–$400\ {\rm cm}^{-3}$. The absolute values of polytropic index Γ increases with decreasing core densities, and varies by about 20% for the adopted range of $T_{\rm c}$ and $(n_{\rm H})_{\rm c}$. We have chosen model 2a as our standard model. We have run chemical models also with other polytropic models, particularly with core densities of $5 \times 10^4\ {\rm cm}^{-3}$ and $10^5\ {\rm cm}^{-3}$. We observed no significant changes in the predicted column densities and overall results, however, in the discussion of the results we will mention those cases where we found noticeable differences, e.g. the effects of higher core density or higher visual extinction on the predicted column density of certain species.

Fig. 1a shows the density, temperature and $A_{\rm v}$ profiles along the radius for the standard model, Fig. 1b shows the cloud structure for two models 1a and 5d, Figs. 1c and 1d show the constant nonthermal (VNT) and the variation of thermal (VT) velocity dispersions with radius for the standard model, and for models 1a and 5d. Note that for all models the nonthermal velocity dispersion is smaller than thermal velocity dispersion except for model 1a (characterised by a lower density of $(n_{\rm H})_{\rm c} = 2 \times 10^4$ ${\rm cm}^{-3}$ at the centre of the cloud), where the nonthermal component dominates close to the centre of the cloud. This difference may indicate that, to satisfy the observed condition of $\Delta v_{\rm NT} < \Delta v_{\rm T}$ a cloud may need to have a density greater than $2 \times 10^4\ {\rm cm}^{-3}$ at the centre of its core.

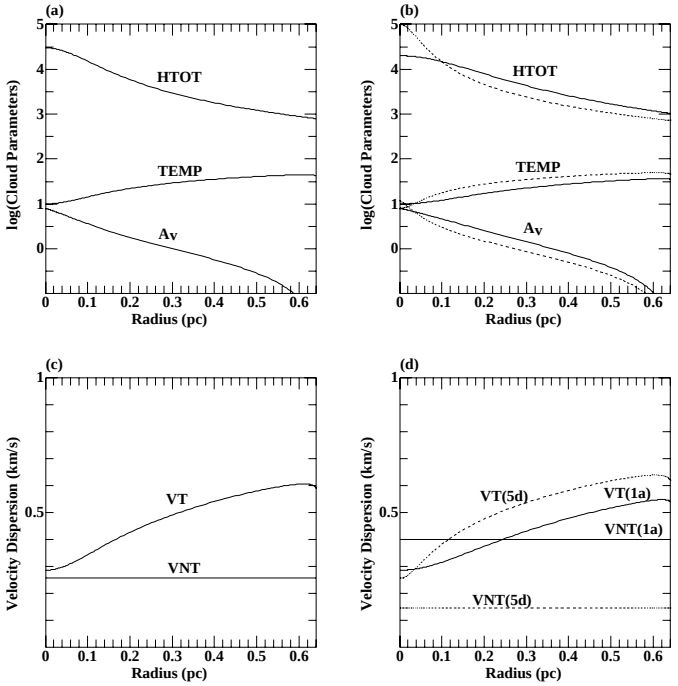

Fig. 1. a Decimal logarithmic variation of temperature (in K), total density (in ${\rm cm}^{-3}$) and $A_{\rm v}$ (in mag) along the radius for the standard model. **b** As in **a**, but showing the profiles for polytropic models 1a (solid lines) and 5d (dashed lines); see Table 1. **c** Variation of thermal velocity component (VT) and the constant nonthermal velocity component (VNT) for the standard model. **d** As in **c**, but showing the velocity components for polytropic models 1a and 5d; see Table 1.

3. Chemical model

The profiles of the physical parameters ($n_{\rm H}(r)$, $T(r)$, $A_{\rm v}(r)$, $f(r)$) obtained from the spherical symmetric polytropic model and the associated initial conditions are used to calculate pseudo-time-dependent chemical abundances for each depth point along the central line of sight; these abundances then can be used to derive the abundances for other lines of sight for the case where we assume an isotropic radiation field. For the simple 2-D model, where the cloud is exposed to a radiation field in the direction of the observer from both sides, the chemical abundances are calculated at each depth point along each line of sight.

For the standard model we have adopted cloud model 2a with a total visual extinction (i.e. $2 \times (A_{\rm v})_{\rm c}$) of 16 mag, and at the centre of the cloud a total hydrogen density of $(n_{\rm H})_{\rm c} = 3 \times 10^4$ ${\rm cm}^{-3}$and a temperature of $T_{\rm c} = 10$ K. Pseudo-time-dependent chemical models have been extensively considered in other studies (Millar & Nejad 1985; Herbst & Leung 1986). The chemical network used in this work consists of 175 species containing H, He, C, O, N, S and Na in a network of about 2100 gas phase reactions extracted from the UMIST Rate95 reaction library (Millar et al. 1997). We have adopted relative to hydrogen cosmic abundances of 0.07, 3.75×10^{-4}, 6.76×10^{-4} and 1.15×10^{-4} for He, C, O and N respectively (Nejad & Williams 1992). The main differences between the elemental abundances used in the

literature for diffuse clouds and dense core models are in the sulphur and metal abundances, both significantly affecting the ionization structure in the cloud. It is generally accepted that high elemental metal abundances are more appropriate for diffuse cloud gas-phase chemistry, whereas low elemental metal abundances are more suited for dense cloud chemistry. Since our model includes both the dense regions and the diffuse envelope surrounding it, we have adopted an intermediate elemental fractional metal abundance of 10^{-7} for Na.

High sulphur abundances have been observed in diffuse ISM; an abundance of about a few$\times 10^{-6}$ is derived from low-resolution *IUE* studies, and about 10^{-5} from high-resolution *HST*-GHRS observations (see Palumbo et al. 1997, and references therein). In chemical models of dense clouds the elemental sulphur abundance has been largely chosen as a free parameter (Millar & Herbst 1990; Lee et al. 1998; Williams 1998) and assumed to be depleted by 2–3 orders of magnitude from the solar abundance. The depleted sulphur is generally assumed to be locked up in icy grain mantles. This assumption is in agreement with IR observations of solid OCS and SO_2 towards dense molecular clouds (Palumbo et al. 1997). These observations imply an upper limit of about 10^{-6} for the total abundance of sulphur-bearing ices. Therefore, it is plausible to assume that the gas phase abundance of sulphur in the cloud core is only about 1% of that in the outer envelope. Based on the observation of sulphur in diffuse interstellar clouds and observations of S-containing ices in dense clouds, considering a constant elemental abundance for sulphur seems to be inadequate for modelling both the diffuse outer region and the dense core of our spherical cloud model. Therefore, in our model we have implemented a density dependent sulphur depletion where the sulphur abundance is inversely proportional to total density $n_{\rm H}(r)$; we assumed a sulphur abundance of 3.2×10^{-6} at the edge of the cloud which decreases with total density by two orders of magnitude to 3.2×10^{-8} at the centre of the cloud.

In all our models the elemental abundances of C, O and N are assumed constant throughout the cloud from surface to core. This assumption is supported by recent results from *HST*-GHRS observations which indicate that there is no significant variation in the gas phase abundances of C, O and N from studies of several lines of sight covering a wide range of extinctions; see Cardelli et al. (1996) for abundance of interstellar carbon, Meyer et al. (1998) for oxygen and Meyer et al. (1997) for nitrogen.

The initial abundances of H and H_2 are depth dependent and are determined by $f = \frac{2n(\rm H_2)}{n_{\rm H}}$, calculated as outlined in Sect. 2.1. The assumed equilibrium between H_2 formation and photodissociation implies that in the outer part of the cloud hydrogen is mostly in atomic form and beyond a depth of about $A_{\rm v} \gtrsim 1$ almost all hydrogen is in molecular form.

We assumed a cosmic-ray ionization rate $\zeta_{\rm cr} = 3 \times 10^{-17}\,{\rm s}^{-1}$ throughout the cloud. Our standard model includes cosmic-ray-induced photoionization and photodissociation reactions using the rates given by Gredel et al. (1989) with a grain albedo $\omega = 0.3$; these rates were scaled to account for the assumed cosmic-ray ionization rate in the model. For CO it is assumed that the CRI photodissociation rate is dependent on the temperature as suggested by Gredel et al. (1989) and adopted by Rawlings et al. (1992). It should be noted that in this paper, for simplicity reasons, we have not treated the CO photodestruction by external UV photons in detail (cf. van Dishoeck & Black 1988) and used the standard photodissociation rate as in UMIST Rate95 reaction network.

In all cases considered it is assumed that the model cloud is exposed to the standard UV radiation field. It should be noted that the direction of the radiation field can significantly affect the predicted beam averaged column densities of species, especially those which are concentrated in the cloud core. We have examined two models: one in which the cloud is subjected to an isotropic radiation field and another where the cloud is exposed to radiation from a single direction. We found that the effect on column densities can be significant along a line of sight with no more than 0.05 pc distance from the centre of the cloud; but for the outer parts of the cloud the difference in the results is more substantial. However, the absolute values of the column densities in the outer regions are small and therefore they do not contribute greatly to the total beam averaged column density values. The simple 2-D chemical model which we developed is based on our spherical symmetric polytropic physical cloud model which we assumed to be exposed to a two sided external UV radiation field in the direction of the observer. We have chosen this geometry for the reason that it produces identical results compared to the other model for the chemical abundances along the central line of sight on which most of our analysis is based.

The models account for the formation of molecular hydrogen through atomic hydrogen recombination on grain surfaces. In addition, since CO is the most abundant molecule after H_2 it can contribute appreciably to mantle growth as suggested by Duley (1974). Therefore, in order to simply examine the effects of gas phase depletion by accretion onto grains, we have included grain accretion only for CO in all models except in one (chemical model B) in which we excluded the loss of CO onto grains in order to assess the accretion effects on the chemistry (see Sect. 4.7 for a discussion). Adopting the grain properties and parameters given by Duley & Williams (1984), Millar & Nejad (1985) and Willacy et al. (1994), we used the following equation for the CO accretion onto grains with time,

$$\frac{{\rm d}n({\rm CO})_{\rm gr}}{{\rm d}t}|_{\rm acc} = 3.2 \times 10^{-17}{\rm cm}^3{\rm s}^{-1}\, n_{\rm H}\, S \left(\frac{T[{\rm K}]}{m_{\rm CO}[{\rm amu}]}\right)^{1/2} n({\rm CO}) \qquad (10)$$

where $n({\rm CO})_{\rm gr}$ is the gas phase equivalent number density of accreted CO, n(CO) is the number density of CO in the gas phase, S is the sticking coefficient and $m_{\rm CO}$ is the molecular mass of CO. It is generally accepted that accreted gas phase matter is, at least, partly returned to the gas phase after being possibly subject to grain surface processes (see Williams 1993, and references therein). Several desorption processes have been suggested - some of these processes are intermittent, appropriate to regions which are subject to periodical disruptions as in the case of high velocity flows and low mass star formation (Charnley et al. 1988; Hartquist et al. 1993; Nejad et al.

1994). For dense cores which show no evidence of star formation, continuous mantle desorption processes have been suggested. Willacy & Williams (1993) have considered two continuous desorption mechanisms - direct cosmic-ray heating of dust grains and cosmic-ray-induced desorption. In another study Willacy et al. (1994) have investigated the effects of a desorption mechanism driven by the energy released from H_2 formation on dust. In order to include a mechanism for CO desorption in our models, we considered the direct cosmic-ray heating of dust grains which seems to be most appropriate for the conditions in dense cloud cores. To implement this process we have adopted a similar formulation to that of Willacy & Williams (1993); assuming small grains (with grain radius $a \sim 0.1\,\mu$), we used for the specific average grain surface the value of

$$\frac{<\pi a^2 n_{\rm gr}>}{n_{\rm H}} = 2.1 \times 10^{-21} \qquad {\rm cm}^2 \tag{11}$$

where $n_{\rm gr}$ is the number density of grains (Duley & Williams 1984). The time variation of the number density of accreted CO due to cosmic-ray spot heating is given by the expression,

$$\frac{{\rm d}n({\rm CO})_{\rm gr}}{{\rm d}t}|_{\rm disorp} = \frac{<\pi a^2 n_{\rm gr}>}{n_{\rm H}}\, \epsilon\, R({\rm CO})\, n_{\rm H} \tag{12}$$

where $\epsilon = 70$ molecules ${\rm cm}^{-2}{\rm s}^{-1}$ is the CO evaporation rate due to spot heating by cosmic-rays, adopted from Léger et al. (1985); for the fraction of the number of mantle layers consisting of solid CO, R(CO), we have adopted, using an estimate from Léger (1983), the following expression,

$$R({\rm CO}) = \frac{n({\rm CO})_{\rm gr}}{3 \times 10^{-6}\, n_{\rm H}} \tag{13}$$

where $n({\rm CO})_{\rm gr}$ is the gas phase equivalent number density of accreted CO. Therefore, the total rate of change of CO on grain mantles with time due to accretion and desorption can be described by the equation,

$$\frac{{\rm d}n({\rm CO})_{\rm gr}}{{\rm d}t} = 3.2 \times 10^{-17}\,{\rm cm}^3{\rm s}^{-1}\, n_{\rm H}\, S \left(\frac{T[{\rm K}]}{m_{\rm CO}[{\rm amu}]}\right)^{1/2} n({\rm CO}) \; - \; 5 \times 10^{-14}\,{\rm s}^{-1}\, n({\rm CO})_{\rm gr} \tag{14}$$

using Eqs. (10) to (13). Our results show that the desorption of CO by cosmic-ray heating is efficient in returning the accreted CO back to the gas phase and produce a closer agreement with observations for the abundances of CO and several other species at the late stages of the cloud evolution. The effects of CO accretion and desorption on gas phase abundances and chemical evolution of the cloud are discussed with results in the following sections.

The effects of cosmic-ray-induced photodesorption can similarly be included, although it is expected to be not as effective as the desorption by direct cosmic-ray heating. For the dense core of a cloud where the density is greater than about $10^4\,{\rm cm}^{-3}$, the H_2 formation timescale is less than $\sim 10^5$ years, therefore a desorption mechanism based on H_2 formation is probably not sufficiently efficient to compete with cosmic-ray heating. However, in the outer and less dense part of the cloud with moderate $A_{\rm v}$ the situation could be reversed and desorption based on H_2 formation might become the dominant desorption process. A thorough study of various desorption mechanisms in the context of depth dependent models may reveal new insights into the proposed gas and dust interaction processes in dense molecular cores.

Finally, we note briefly some of the computational aspects. During the development of this paper, we have extensively upgraded the differential rate equation writer DELOAD (Nejad 1986; Bennett 1988). The new code, XDELOAD Version 98, is an Xwindows application which uses dynamic memory allocation. This greatly reduces the number of settings that the user must adjust, and eliminates program errors due to inadequate sizing of arrays. The new program design greatly simplifies the usage of the code and reduces the user inputs to the absolute necessary level, i.e. the only inputs required are the species and the reaction files. All sorting is performed automatically by selecting appropriate icons. The complete description including installation and usage supplemented with example files and a test program is available on the Internet. Integrations were performed using the VODE ordinary differential equation solver package (Brown et al. 1989) and the computations were carried out on an INDY Silicon-Graphics workstation.

4. Results and discussions

The model results given here are not representative of any particular dense molecular cloud; however, with the physical and chemical assumptions adopted in this work, it seems reasonable to compare our results with observations of dark molecular cloud complex TMC-1, particularly because of the relatively large amount of data available for TMC-1.

For presenting our chemical results we selected mainly three groups of species; the first group contains those species whose peak abundances are reached at the so-called "early times", i.e. observed nitrogen and sulphur containing carbon-chain molecules and related hydrocarbons, namely HC_3N, C_2S, C_3H_2 and related species. This group of species is of special interest because of recent observational studies (Hirahara et al. 1992; Suzuki et al. 1992) suggesting a chemical correlation between these molecules which are termed as "acetylenic" species by Turner et al. (1998) in their combined observational/theoretical studies of these molecules in small translucent clouds. We also consider the chemistry of the CH_3CN and CH_3OH which are most critically affected by the influence of cosmic-ray-induced photoionization and photodissociation processes and their chemical evolution is confined to the early times. The second group of species include CS (with HCS^+) and CO (with HCO^+) which are extended both with respect to time and depth into the cloud. The third set of species are those which reach their maximum abundances at "later times" of the cloud evolution, namely NH_3, N_2H^+ and SO. In addition, we consider the overall effects of cosmic-ray-induced photons on the chemistry at early times, and effects of CO accretion and desorption on the chemistry of species at late times of the cloud evolution. The effects of CO accretion becomes

apparent at times $\gtrsim 2 \times 10^5$ years and the desorption process becomes significant after $\sim 10^6$ years. Therefore, to allow reasonable comparisons with other works in all tables of results we list abundances and column densities corresponding to three different evolution times of 2×10^5, 5×10^5 and 10^6 years.

Initially, all elements are assumed to be in atomic form except for hydrogen where the fraction of H_2 is defined by the ratio $f = \frac{2n(H_2)}{n_H}$, as calculated in Sect. 2.1. It is important to note that the assumed initial H/H_2 ratio significantly affects the computed abundances at early times. Our results indicate that abundances of a large number of species can vary by 2 orders of magnitudes at times $\lesssim 10^4$ years depending on whether initially hydrogen is assumed all in atomic or all in molecular form. However, this difference becomes insignificant at times $\gtrsim 10^5$ years, leading to identical steady-state solutions.

We have also run our standard model with two different sets of elemental abundances for C, O and N, one using solar elemental abundances of Grevesse & Noels (1993), i.e. abundances of 3.55×10^{-4}, 7.41×10^{-4} and 9.33×10^{-5} for C, O and N respectively, and one using new interstellar cosmic elemental abundances derived using *HST*-GHRS observations, i.e. 2.4×10^{-4} for C (Cardelli et al. 1996), 5.0×10^{-4} for O (Meyer et al. 1998) and 7.5×10^{-5} for N (Meyer et al. 1997). Using these two sets of elemental abundances for C, O and N, we found in both cases, compared with our standard model results, neither a significant change in the structure of the chemistry nor differences greater than about a factor of two in the calculated column densities of certain species at about 10^6 years. These model results approximately scale with the chosen elemental abundances while the C/O ratio is preserved.

Another related issue is the dependence of the steady-state solutions to the initial chemical composition of the cloud for elements other than hydrogen. We examined our models by assuming all C, O and N initially in the form of CO, O_2 and N_2 , respectively (cf. Lee et al. 1998). Steady-state solutions remain largely unchanged for abundant species including electron abundances; for species with very low abundances we found steady-state solutions are no more than a factor of three different using these two choices of initial chemical composition.

There have been some investigations in recent years in possible bistable steady-state solutions of chemical rate equations in astrochemical cloud modelling (Pineau des Forêts et al. 1992; Le Bourlot et al. 1995a, b; Lee et al. 1998). It is known that if one takes a different set of initial conditions and control (physical) parameters then it is possible for a (highly) non-linear system of ordinary differential equations to reach a different steady-state solution. This phenomenon is known as multistability or multiplicity of stationary-state solutions. Furthermore, in general, if a system is multistable then bistable behaviour is also possible. The essential ingredients for bistability are nonlinearity and feedback (or history of the system) (Epstein 1990; Scott 1994). Bistability (hysteresis) is highly dependent upon the choice of parameters and can be seen in such a system of rate equations by increasing and then decreasing one of the parameters (using the solution for one parameter value as the initial condition for the system at the next parameter value). Recently, Lee et al. (1998) using the new neutral-neutral reaction network of Bettens et al. (1995) have shown that over a certain range of densities it is possible to find a multistable region, within which they found two steady-state solutions, obtained by choosing two different initial chemical compositions for O, C and N, i.e. atomic and molecular initial conditions. We have examined several models using the elemental abundances and initial conditions adopted by Lee et al. (1998), except that we used in our models a variable temperature, variable A_v and the reaction network UMIST Rate95. For all the examined models we were unable to find any abrupt jump (or bifurcation) in the steady-state solutions within the parameter window used by Lee et al. (1998). In particular, their results indicate that sulphur depletion is a key parameter for the presence of multiple steady-state solutions. We have not found such a sensitivity of our model results to the choice of sulphur depletion. The main difference between the existence and non-existence of multiple steady-state solutions, thus, relies largely on the reaction network utilized; a conclusion that was also reached by Lee et al. (1998).

Observationally there are errors in deriving column densities and abundances. Pratap et al. (1997) suggested that there are less uncertainties in deriving abundances than column densities. Considering possible observational uncertainties (e.g. in measurement and calibration) in deriving abundances they showed that if the errors are uncorrelated, then the relative abundances could have an uncertainty of approximating 20%. Likewise, accuracy is higher in theoretical modelling when calculating abundances compared to column densities. We believe that the uncertainties in using various numerical routines (integrations and interpolations) required in calculating column densities should result in no more than approximating 10% uncertainty due to computational errors provided that high order accuracy numerical techniques are adopted. However, column densities allow a more direct and meaningful comparison with observations and provide additional information for the interpretation of results.

To allow comparison with time dependent chemical models and observations we present results for a selected number of species in various forms: the time variation of molecular abundances in the centre of the cloud, the variations of molecular abundances with radius and A_v for a number of species at selected times, the variation of column densities with time along the central line of sight and average column densities corresponding to various sizes of a telescope beam centred at the centre of the cloud. The results for the standard model, Model A (no CRI photoionization) and Model B (no CO accretion) are shown in Figs. 2–5. The predicted column densities for the central line of sight and the corresponding column densities for various beam sizes are listed in Table 2. The predicted abundances of several species along the central line of sight are listed in Table 3 for the selected evolution times and for various local A_v. The results corresponding to Table 2 and Table 3, but using a lower sticking coefficient for the CO accretion rate are listed in Table 4 and Table 5, respectively. Table 6 lists the results corresponding to Table 2, but for our simple 2D model where it is assumed the cloud is exposed to a radiation field in the direction of the observer from both sides.

4.1. HC_3N, C_3H_2 *and* C_2S

From the observational survey of dense cloud cores, Suzuki et al. (1992) reported a close correlation in HC_3N and C_2S column density distributions, and noted a weaker correlation between abundances of C_3H_2 and HC_3N. The production chemistry of C_3H_2 is known to be related to those of carbon-chain molecules (Adams & Smith 1987). The chemistry of HC_3N and C_2S are also related through their connections to the hydrocarbon chemistry. In order to study the chemistry of this group of species and their relations, we consider them in detail in the following sections.

4.1.1. HC_3N

Cyanoacetylene is among the best studied species in dark clouds. It is known that HC_3N is abundant at the early times of the cloud evolution in contrast to NH_3 which becomes more abundant at later times. Our models show that HC_3N abundance peaks at about 3×10^5 years and is well connected to the hydrocarbon chemistry. An analysis of the chemistry in the standard model indicates that in the vicinity of the centre of the cloud the following sequence of reactions is most efficient for the formation of HC_3N at $t \lesssim 10^4$ years,

$$\begin{aligned}\mathrm{C} \xrightarrow{\mathrm{H_3^+}} \mathrm{CH^+} \xrightarrow{\mathrm{H_2}} \mathrm{CH_2^+} \xrightarrow{\mathrm{H_2}} \mathrm{CH_3^+} \xrightarrow{\mathrm{C}} \mathrm{C_2H^+} \xrightarrow{\mathrm{H_2}} \mathrm{C_2H_2^+} \\ \xrightarrow{\mathrm{C}} \mathrm{C_3H^+} \xrightarrow{\mathrm{H_2}} \mathrm{C_3H_3^+} \xrightarrow{\mathrm{e}} \mathrm{C_3H_2} \xrightarrow{\mathrm{N}} \mathrm{HC_3N} \end{aligned} \quad \text{(R1)}$$

During the period of high production, $10^4 \lesssim t \lesssim 6 \times 10^5$, the formation of HC_3N is dominated by another reaction sequence involving C_3H and C_3N,

$$\mathrm{C_3H} \xrightarrow{\mathrm{N}} \mathrm{C_3N} \xrightarrow{\mathrm{H_3^+}} \mathrm{HC_3N^+} \xrightarrow{\mathrm{e}} \mathrm{H_2C_3N^+} \xrightarrow{\mathrm{e}} \mathrm{HC_3N} \quad \text{(R2)}$$

where C_3H is produced at all times through the sequence,

$$\begin{aligned}\mathrm{C} \xrightarrow{\mathrm{H_3^+}} \mathrm{CH^+} \xrightarrow{\mathrm{H_2}} \mathrm{CH_2^+} \xrightarrow{\mathrm{H_2}} \mathrm{CH_3^+} \xrightarrow{\mathrm{C}} \mathrm{C_2H^+} \\ \xrightarrow{\mathrm{H_2}} \mathrm{C_2H_2^+} \xrightarrow{\mathrm{H_2}} \mathrm{C_2H_4^+} \xrightarrow{\mathrm{e}} \mathrm{C_2H_2} \xrightarrow{\mathrm{C}} \mathrm{C_3H} \end{aligned} \quad \text{(R3)}$$

From the centre of the cloud to a moderate depth of $A_\mathrm{v} \sim 5$ mag, very similar reaction sequences involving hydrocarbons dominate the production of HC_3N at all times. However, with decreasing A_v, HC_3N is produced mostly via reaction sequence (R1) involving directly C_3H_2, and reaction sequence (R2) is only dominant shortly at about the peak abundance time of HC_3N, $t \sim 3 \times 10^5$ years. Furthermore, in the standard model at $A_\mathrm{v} \sim 4$ mag, the contribution from reaction sequence (R2) to the production of HC_3N becomes less important; instead in these intermediate A_v regions, where sulphur is not yet greatly depleted, at time $t \gtrsim 2\times10^5$ years another sequence of reactions, directly connected to carbon chain sulphur-containing species and C_3H_2, becomes the major source of HC_3N production,

$$\begin{aligned}\mathrm{C_3H} \xrightarrow{\mathrm{S^+}} \mathrm{C_3S^+} \xrightarrow{\mathrm{e}} \mathrm{C_2S} \xrightarrow{\mathrm{C^+}} \mathrm{C_3^+} \xrightarrow{\mathrm{H_2}} \mathrm{CH_3^+} \\ \xrightarrow{\mathrm{H_2}} \mathrm{C_2H_3^+} \xrightarrow{\mathrm{e}} \mathrm{C_3H_2} \xrightarrow{\mathrm{N}} \mathrm{HC_3N} \end{aligned} \quad \text{(R4)}$$

Note that the above route to the formation of HC_3N via C_2S is important only in the standard model in the presence of cosmic-ray-induced photons and our analysis of the chemistry showed that such a route for the formation of HC_3N does not exist in Model A, in the absence of CRI photoionization/dissociation reactions. In the inner parts of the cloud, confined to an $A_\mathrm{v} \gtrsim 3$ mag, the most effective process for the production of C^+ is CRI photoionization of atomic C; furthermore, the subsequent reaction of C^+ with atomic sulphur dominates the production of S^+,

$$\mathrm{C} \xrightarrow{\mathrm{CRI}} \mathrm{C^+} \xrightarrow{\mathrm{S}} \mathrm{S^+} \quad \text{(R5)}$$

At A_v lower than about 3 mag, photoionization of C by external UV photons becomes the dominant production source of C^+.

The observed column density of HC_3N toward TMC-1 is in the range of $(6\text{–}17)\times10^{13}$ cm^{-2} (Ohishi et al. 1992; Hirahara et al. 1992; Suzuki et al. 1992; Pratap et al. 1997). Our model results show that for the central line of sight the column density of HC_3N peaks at $\sim 3\times10^5$ years, with a value of $1.1\times10^{14}\mathrm{cm}^{-2}$, which is in good agreement with observations. The chemistry of HC_3N involves a large number of hydrocarbons and, except for a few key neutral-neutral reactions its production is critically dependent on ion-molecule and electron recombination reactions. Thus the abundance of HC_3N is strongly influenced by the ionization level in the cloud. In order to investigate further the influence of the fractional ionization on the HC_3N chemistry, we excluded in Model A cosmic-ray-induced photoionization and photodissociation reactions. We found that in Model A, in the absence of CRI photons, reaction sequence (R2) is the dominant reaction chain for the production of HC_3N at higher A_v ($\gtrsim 4$ mag) at all times $t \gtrsim$ few$\times10^3$ years and, unlike the standard model, the formation of HC_3N is not directly linked to C_3H_2 nor to sulphur-containing carbon chain molecules.

As can be seen in Fig. 2e, the difference between the predicted column density of HC_3N in the two models is much greater at the earlier times due to the influence of the cosmic-ray-induced reactions which are more significant at earlier times. For example, at about 10^5 years, the predicted column density of HC_3N is about an order of magnitude higher in Model A than the corresponding value predicted by the standard model. This difference in the abundances of HC_3N decreases to about a factor of 2 at around 6×10^5 years; at later times the predicted abundances of HC_3N of both models are almost identical. This result indicates that in the absence of additional photons either the production of HC_3N is more efficient or it is lost at a slower rate. In the standard model at $A_\mathrm{v} \gtrsim 4$, and for times less than about 10^6 years, about 80% of the loss of HC_3N is due to reaction with C^+ and about 15% by reactions with other abundant ions. In the standard model the source of C^+ in denser regions is mainly cosmic-ray-induced photoionization of atomic C, and at later times via CO reaction with He^+ through the reaction,

$$\mathrm{CO + He^+ \rightarrow C^+ + He + O} \quad \text{(R6)}$$

In the absence of CRI photons, about half of the loss of HC_3N at early times is via reaction with C^+, and the remaining loss is via

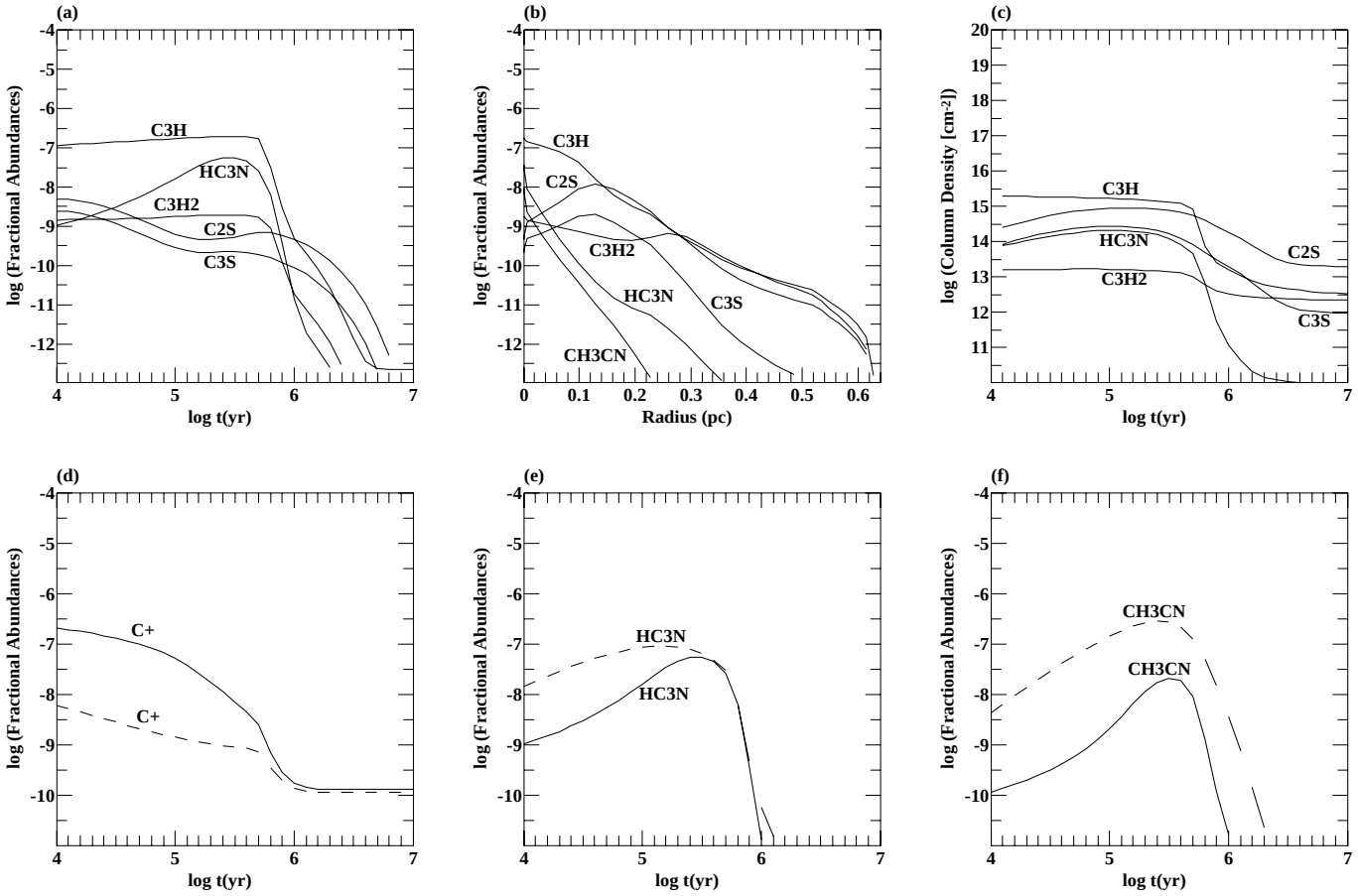

Fig. 2. a Time variation of fractional abundances corresponding to the centre of the cloud. **b** Variation of fractional abundances with radius from the centre of the cloud at $t = 2 \times 10^5$ years. **c** Time variation of integrated column densities (along the central line of sight. **d** Fractional abundances of C^+ for the standard model (solid line) and in the absence of cosmic-ray-induced photoionization/dissociation effects (dash line). **e** As in **d**, but for fractional abundance of HC_3N. **f** As in **d**, but for fractional abundance of CH_3CN.

reactions with other major ions. At later times, when sufficient H_3^+ becomes available (due to the loss of CO from the gas phase – see Sect. 4.7), the loss of HC_3N via reaction with H_3^+ becomes more effective compared to the destruction reaction with C^+. In the outer parts of the cloud with an $A_v \sim 3$ the loss through UV photodissociation becomes dominant over the loss by reaction with C^+. In Model A, C^+ is formed through reaction (R6) at higher A_v, and through photoionization of atomic C by the external UV photons at lower A_v. By comparing the absolute values of the production and destruction contributions to the abundance of HC_3N we found that in both models the magnitude of the total production rates has the same order. However, in the absence of additional CRI photons the loss of HC_3N is at least one order of magnitude smaller than the loss in the standard model; hence faster destruction of HC_3N in the standard model, due to the larger abundance of C^+, explains the lower predicted abundance of HC_3N. Similar results regarding the sensitivity of the HC_3N abundance to the fractional ionization level were found by changing the assumed A_v or the adopted ζ_{cr}.

The anticorrelation between C^+ and HC_3N abundances at early times, when the ionization level in the cloud core is substantially higher than at late times, is very apparent in Figs. 2d and 2e. Fig. 2b shows that the radial extent of HC_3N is limited to a narrow region about 0.1 pc from the centre of the cloud core. This is in agreement with the observed small extent of the HC_3N emission, indicating that a slight offset from the peak of the HC_3N distribution might be enough to account for the apparent weakness of HC_3N toward many dark cores (Fuller & Myers 1993). This effect can be seen in Fig. 3d, which shows the large difference between the predicted peak column density of HC_3N along the central line of sight and the corresponding average column density of HC_3N integrated over a beam size of 0.1 pc. Such an effect applies to a number of molecules (e.g. CH_3CN and SO) whose column densities vary critically with depth (as well as with time).

4.1.2. C_3H_2

In sequence (R1), the final reaction between C_3H_2 and N shows a direct connection between HC_3N and C_3H_2. The production chemistry of C_3H_2 also closely links the hydrocarbon chemistry with carbon-chain molecules (Adams & Smith 1987). Sequence (R1) clearly explains the positive correlation between column densities of HC_3N and C_3H_2 found in the observational survey

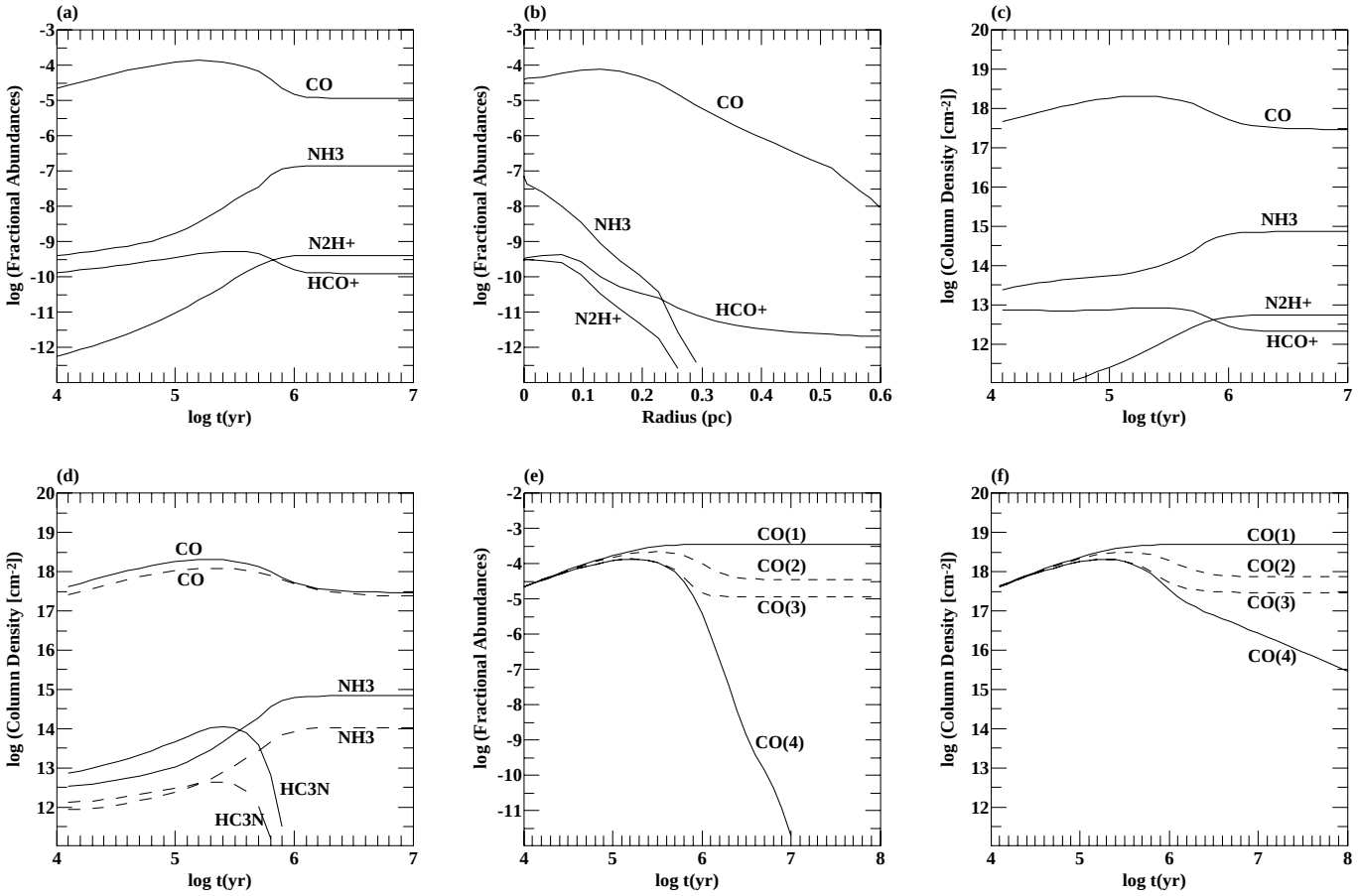

Fig. 3. a Time variation of fractional abundances corresponding to the centre of the cloud. **b** Variation of fractional abundances with radius at $t = 10^6$ years. **c** Time variation of integrated column densities along the central line of sight. **d** Comparison between the time variation of integrated column densities along the central line of sight (solid lines) and time variation of average column densities integrated over a beam radius of 0.1 pc (dash lines). **e** Time variation of fractional abundances of CO in the case of no accretion - CO(1), CO accretion with a sticking coefficient of 0.1 and desorption - CO(2), CO accretion with a sticking coefficient of 0.33 and desorption - CO(3) and CO accretion with a sticking coefficient of 0.33 and no desorption - CO(4). **f** As **e**, but showing the time variation of the CO column density for the central line of sight.

of dark cloud cores by Suzuki et al. (1992). The correlation between C_2S, HC_3N and C_3H_2 was recently investigated by Turner et al. (1998) in the context of small translucent clouds, where, however, the necessary conditions for such a correlation are only weakly satisfied.

The relation of C_3H_2 and HC_3N at early times is due to effective production of HC_3N by the key neutral-neutral reaction between C_3H_2 and atomic N which also provides the most effective loss reaction for C_3H_2. From examining the HC_3N chemistry above, we can conclude that the observed correlation between C_3H_2 and HC_3N can effectively exist in the presence of higher ionization fractions; in the case of this study, the cosmic-ray-induced ionization provides the source of additional photons in the denser part of the cloud.

The chemistry of C_3H_2 establishes at early stages of the cloud evolution and its peak column density of $2.4 \times 10^{13}\ \mathrm{cm}^{-2}$ is reached at $\sim 10^4$ years; this column density decreases only by a factor of two until about 6×10^5 years (see Fig. 2a). During the early period of rapid production, C_3H_2 provides the most efficient formation route for HC_3N. In addition, C_3H_2 provides also the main formation source of HC_3N at lower extinctions; this effect can be seen in Fig. 4a, which displays the depth variation of abundances of C_3H_2 and HC_3N. The chemistry of C_3H_2 in Rate95 (Millar et al. 1997) has only two production reactions, i.e. electron recombination of $C_3H_3^+$ and photodissociation of C_3H_3; our analysis shows that the latter reaction makes no contribution to the production of C_3H_2 at all depths and times. The C_3H_2 distribution is extended, both with respect to time and depth into the cloud; it is similar to that of CO. The C_3H_2 abundance distribution and the column density variation, with respect to space and time, can be seen in Figs. 2b and 2c respectively. The predicted abundance of C_3H_2 changes only by a factor of a few from the core to the outer parts of the cloud where $A_\mathrm{v} \sim 2$ mag (see Fig. 4a). This is in agreement with observations of C_3H_2 toward dark clouds as well as diffuse clouds with a measured column density of few$\times(10^{12} - 10^{13})\ \mathrm{cm}^{-2}$ which is quite comparable in both types of clouds. Our predicted maximum column density of $2.4 \times 10^{13}\ \mathrm{cm}^{-2}$ is within a factor of

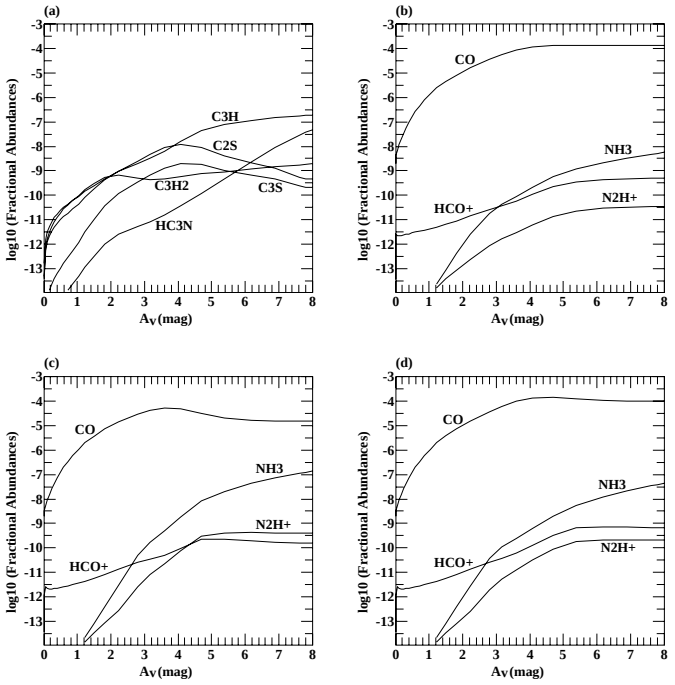

Fig. 4. a Variation of fractional abundances with radius at $t = 2 \times 10^5$ years for the standard model. **b** As in **a**, but for CO, HCO^+, NH_3 and N_2H^+. **c** As in **b**, but at $t = 10^6$ years. **d** As in **c**, but for model B (i.e. CO sticking coefficient = 0.1).

2 in good agreement with the measured value of $\sim$ 3–4 $\times 10^{13}$ cm^{-2} reported recently by Ohishi & Kaifu (1998). Our models predict a C_3H_2 column density of about 10^{12} cm^{-2} for the outer parts of the cloud where $A_\mathrm{v} \sim 1$ mag. This is in agreement with measurements of about 5×10^{12} cm^{-2} from diffuse cloud observations (Cox et al. 1988). Our calculated peak fractional abundance of $\sim 2 \times 10^{-9}$ at the centre of the cloud is within a factor 3 in agreement with the measured abundance of $\gtrsim 5 \times 10^{-9}$ (Matthews & Irvine 1986).

4.1.3. C_2S

C_2S and C_3S form another series of carbon-chain molecules which since their laboratory detections (Saito et al. 1987; Yamamoto et al. 1987) have been subject of several observational (Hirahara et al. 1992; Suzuki et al. 1992; Wolkovitch et al. 1997; Peng et al. 1998) and theoretical studies (Smith et al. 1988; Millar & Herbst 1990; Howe et al. 1996). The production of C_2S in the centre of the standard model cloud, at times $t \lesssim 2 \times 10^5$ years, is dominated by the following reaction chain,

$$\mathrm{C_3H} \xrightarrow{\mathrm{C^+}} \mathrm{C_4^+} \xrightarrow{\mathrm{H_2}} \mathrm{C_4H^+} \xrightarrow{\mathrm{H_2}} \mathrm{C_4H_2^+} \xrightarrow{\mathrm{e}} \mathrm{C_4H} \xrightarrow{\mathrm{S^+}} \mathrm{C_4S^+} \xrightarrow{\mathrm{e}} \mathrm{C_2S} \qquad \text{(R7)}$$

where C_3H is formed via reaction sequence (R3). At about $t \gtrsim$ 2–4 $\times 10^5$ years, corresponding to the peak abundance time of "early type" species, the following reactions becomes most effective in the formation of C_2S,

$$\mathrm{C_3H} \xrightarrow{\mathrm{S^+}} \mathrm{C_3S^+} \xrightarrow{\mathrm{e}} \mathrm{C_2S} \qquad \text{(R8)}$$

Here it should be noted that the sulphur abundance in the centre of cloud is reduced by 2 orders of magnitude from the abundance assumed at the edge of the cloud and therefore, the contribution of the centre of the cloud to the large predicted column density of C_2S is not substantial. In fact the largest contribution to the total column density of C_2S is attributed to the region with an $A_\mathrm{v} \sim$ 6–4 mag; in this region the most dominant formation route, at all effective production times, is the sequence (R8). At $A_\mathrm{v} \lesssim 3$ mag the formation of C_2S is dominated by the sequence,

$$\mathrm{S} \xrightarrow{\mathrm{C^+}} \mathrm{C_2H} \xrightarrow{\mathrm{S^+}} \mathrm{C_2S^+} \xrightarrow{\mathrm{H_2}} \mathrm{HC_2S^+} \xrightarrow{\mathrm{e}} \mathrm{C_2S} \qquad \text{(R9)}$$

where C^+ and S^+ are produced via photoionization by the external UV photons. The reaction sequences (R7) and (R1) clearly show that the production chemistry of C_2S and HC_3N are dominated by hydrocarbon chemistry particularly that of C_3H. Since the S^+ ion does not react with H_2 in dark clouds (Prasad & Huntress 1980), it is available to react with hydrocarbons which dominate the production reactions for HC_3N and C_2S. Reaction sequence (R8), shows that the reaction between C_3H and S^+ produces the precursor ion C_3S^+ for the production of C_2S. In addition to C_3S^+ and C_4S^+, $HC_{2,3,4}S^+$ ions contribute to the production of C_2S. The formation route for all these ions is through various reactions involving abundant hydrocarbons like, C_2H_2, C_3H and C_4H, with S^+ and reactions of hydrocarbon ions with atomic S.

At about 3×10^5 years, corresponding to the peak abundance time of HC_3N, our predicted column density of C_2S along the central line of sight is 10^{14} cm^{-2} (see Fig. 2c). This is in good agreement with the measured value of $\sim 10^{14}$ cm^{-2} derived by Hirahara et al. (1992) toward TMC-1 near the so called cyanopolyynes peak.

Other reported observed C_2S column densities include a value of 6.6×10^{13} cm^{-2} derived by Suzuki et al. (1992) and $\sim 8 \times 10^{13}$ cm^{-2} reported by Ohishi et al. (1992) and Ohishi & Kaifu (1998). Wolkovitch et al. (1997) reported a low C_2S column density of 3.3×10^{13} cm^{-2} toward TMC-1D, which is known to be a more evolved clump, and therefore this value fits better with our predicted value of about 3×10^{13} cm^{-2} at $\sim 2 \times 10^6$ years when the ammonia reaches its peak abundance. Our predicted column density of C_3S is $\sim 1.6 \times 10^{13}$ cm^{-2} at 3×10^5 years. In all our models, from the centre of the cloud up to a radius of about 0.2 pc, at times $\sim$ 2–6 $\times 10^5$ years, we found only a small variation in the abundance ratio of C_2S/C_3S $\sim$ 3–4, as can be seen in Fig. 2b; this is in good agreement with the observed abundance ratio of $\sim$ 4 found by Suzuki et al. (1992).

One of the most significant results related to the C_2S and C_3S chemistry, is the effect of cosmic-ray-induced ionization which critically changes the predicted column densities of these carbon-chain sulphur-containing species. In order to understand the changes in chemistry we have also studied the chemical

production reactions of C_2S with Model A, in which the effects of the cosmic-ray-induced reactions are excluded. During the high production times and at higher $A_v \gtrsim 4$ mag, most dominant production routes are via abundant hydrocarbons, followed by reaction with S^+ resulting in the production of the precursor ions, i.e.

$$C_4H \xrightarrow{S^+} C_4S^+ \xrightarrow{e} C_2S \quad \text{(R10)}$$

and

$$C_3H \xrightarrow{S^+} C_3S^+ \xrightarrow{e} C_2S \quad \text{(R11)}$$

At later times the production of C_2S via hydrocarbons becomes less efficient, due to the loss of carbon (by CO accretion onto grains) from the gas phase, and the chemistry of the C_2S becomes limited to the recycling sequence,

$$C_2S \xrightarrow{C^+} C_2S^+ \xrightarrow{H_2} HC_2S^+ \xrightarrow{e} C_2S \quad \text{(R12)}$$

where in the above reactions S^+ is formed via the charge exchange reaction of atomic sulphur and C^+ at all times $t \lesssim 8\times10^5$ years. At later times S^+ is mainly formed via reaction between CS and He^+.

As discussed in the case of HC_3N, the main difference between the standard model and Model A, as far as the chemistry of C_2S is concerned, is due to an increase in the abundance of C^+ in the standard model. In the absence of cosmic-ray-induced photons, depending on the assumed sulphur abundance in the core the predicted column density of C_2S is a factor of 5–10 higher than the measured values, similar to the case of HC_3N.

4.2. CH_3CN

The abundance of CH_3CN is most critically affected by the influence of cosmic-ray-induced ionization on the chemistry. The predicted maximum column density of CH_3CN is reached approximately about the same time as that of HC_3N; therefore it can be grouped as one of the "early type" species. As shown in Fig. 2b, the spatial extent of CH_3CN is particularly small; confined to a radius of about 0.05 pc from the centre of the cloud. In addition to a rapid decrease with radius, the CH_3CN abundance also varies strongly with time. Therefore, in order to allow meaningful comparison with observations, it is essential to know whether the observed column densities have been measured toward the cyanopolyynes or ammonia peak abundances. In the standard model the predicted peak column density of CH_3CN is about a few$\times10^{13}$ cm^{-2} which within a factor of 2–3 is in good agreement with the observed values in the range of $(5\text{–}10)\times10^{12}$ cm^{-2} (Ohishi et al. 1992; Minh et al. 1993). In Model A, in the absence of cosmic-ray-induced photoionization, the maximum predicted column density peaks is about 2×10^{15} cm^{-2}, almost two orders of magnitude higher than the observed value. In order to understand this large discrepancy we analysed the chemistry in the standard model. The most dominant sequences for the production of of CH_3CN are, at times $t \lesssim 5\times10^4$ years,

$$C \xrightarrow{H_2} CH_2 \xrightarrow{N} HCN \xrightarrow{CH_3^+} H_4C_2N^+ \xrightarrow{e} CH_3CN \quad \text{(R13)}$$

and during the times $\sim 6\times10^4 - 5\times10^5$ years,

$$C_3H \xrightarrow{N} C_3N \xrightarrow{H_3^+} HC_3N^+ \xrightarrow{H_2} HCN \xrightarrow{CH_3^+} H_4C_2N^+ \xrightarrow{e} CH_3CN \quad \text{(R14)}$$

where C_3H is formed via sequence (R3). Finally, at later times of $\gtrsim 6\times10^5$ years CH_3CN reaches its equilibrium abundance while locked in recycling reaction sequence,

$$CH_3CN \xrightarrow{H_3^+} H_4C_2N^+ \xrightarrow{e} CH_3CN \quad \text{(R15)}$$

In Model A, although very different abundances are obtained and the maximum column density is shifted to an earlier time of 2×10^5 years, the production sequences overall are very similar to the standard model; i.e. in both models CH_3CN is formed via electron recombination of $H_4C_2N^+$ following reactions involving HCN. The prime difference, similar to the case of the HC_3N chemistry considered above, is the much reduced C^+ abundance due to the smaller ionization fraction in Model A; thus resulting in a decrease in the loss of HCN via reaction with C^+ by approximately one order of magnitude. In the standard model, the C^+ ions involved in the formation of hydrocarbons connected to the chemistry of CH_3CN are formed largely by cosmic-ray-induced photoionization of atomic C during the early times of the cloud evolution, whereas in Model A, the main formation reaction for C^+ is via reaction of CO and He^+. In the standard model the loss of CH_3CN is almost entirely by reaction with C^+ (i.e. $CH_3CN + C^+ \rightarrow C_2H_3^+ + CN$). In Model A, in addition to the loss by reaction with C^+, the destruction via reactions with H_3^+ and H_3O^+ contributes greatly to the loss of CH_3CN, particularly at later times. By comparing the total values of the rate of production and destruction of CH_3CN using the abundances at the centre of the cloud at various times, we found that in the standard model (where the predicted column density is lower) the rate of the loss processes is about a factor of two higher, and the production rate is more than one order of magnitude lower than the corresponding values in Model A. Therefore, a faster destruction and a slower production, due to the higher C^+ abundance, explains the drastic difference in the predicted abundances of CH_3CN between the two models. Fig. 2f displays the effects of cosmic-ray-induced photons, through an increase in the C^+ abundance, on the calculated abundance of CH_3CN. Note that the difference in the abundances is most enhanced at the centre of the cloud and that with increasing radius, as the effects of cosmic-ray-photons are reduced, the difference in abundances decreases between the two models. It is worth noting that, similar to CH_3CN, the abundance of CH_3OH is also significantly affected by cosmic-ray-induced additional photons. The predicted column density in the standard model is in close agreement with observations as shown in Table 2.

4.3. CS *and* HCS^+

Our predicted column density of CS in the standard model at the centre of the cloud is about 4–8 $\times 10^{15}$ cm^{-2} which is 1–2

Table 2. Average column densities (in cm^{-2}) of selected species for various beam-radii (in pc) and evolution times (2×10^5, 5×10^5 and 1×10^6 years) in the standard model; $\bar{A}_\mathrm{v}$ is the beam-averaged total A_v. Note: $x(y)$ refers to $x \times 10^y$.

beam-radius [pc]	0.00	0.02	0.05	0.10	0.15	0.20	0.25	0.30	TMC-1
$\bar{A}_\mathrm{v}$ [mags]	8.0	7.9	7.5	6.5	5.4	4.6	3.9	3.3	
C	4.5 (18)	4.5 (18)	4.5 (18)	4.4 (18)	3.9 (18)	3.2 (18)	2.6 (18)	2.1 (18)	
	2.9 (18)	2.9 (18)	3.0 (18)	3.4 (18)	3.4 (18)	2.9 (18)	2.4 (18)	1.9 (18)	$1-10\,(17)$ [1]
	2.4 (18)	2.4 (18)	2.4 (18)	2.7 (18)	3.0 (18)	2.7 (18)	2.3 (18)	1.8 (18)	
CO	2.1 (18)	2.1 (18)	1.8 (18)	1.2 (18)	6.9 (17)	4.0 (17)	2.8 (17)	1.9 (17)	
	1.4 (18)	1.3 (18)	1.2 (18)	9.5 (17)	5.4 (17)	3.2 (17)	2.2 (17)	1.5 (17)	$8-12\,(17)$ [2]
	5.3 (17)	5.3 (17)	5.3 (17)	5.1 (17)	3.4 (17)	2.1 (17)	1.5 (17)	1.0 (17)	
H_2CO	6.7 (14)	5.4 (14)	2.7 (14)	1.0 (14)	4.6 (13)	2.5 (13)	1.7 (13)	1.2 (13)	
	4.2 (14)	3.3 (14)	2.0 (14)	8.2 (13)	3.7 (13)	2.0 (13)	1.4 (13)	9.2 (12)	5 (14) [8]
	2.5 (13)	2.2 (13)	2.0 (13)	1.8 (13)	9.2 (12)	5.2 (12)	3.5 (12)	2.4 (12)	
HCO^+	4.9 (12)	4.7 (12)	3.5 (12)	1.7 (12)	8.5 (11)	5.0 (11)	3.5 (11)	2.4 (11)	
	5.7 (12)	5.5 (12)	4.5 (12)	2.1 (12)	1.0 (12)	5.8 (11)	4.0 (11)	2.8 (11)	$2-4\,(13)$ [2]
	2.6 (12)	2.6 (12)	2.4 (12)	1.4 (12)	6.9 (11)	4.1 (11)	2.9 (11)	2.0 (11)	
CH	1.1 (15)	1.0 (15)	1.0 (15)	1.1 (15)	1.1 (15)	1.1 (15)	1.1 (15)	1.0 (15)	
	8.5 (14)	8.5 (14)	8.6 (14)	9.1 (14)	9.7 (14)	1.0 (15)	9.7 (14)	8.8 (14)	2 (14) [3]
	7.7 (14)	7.7 (14)	7.8 (14)	8.4 (14)	9.1 (14)	9.5 (14)	9.2 (14)	8.4 (14)	
C_2H	1.3 (14)	1.3 (14)	1.3 (14)	1.3 (14)	1.3 (14)	1.2 (14)	1.2 (14)	1.0 (14)	
	9.5 (13)	9.5 (13)	9.6 (13)	1.0 (14)	1.1 (14)	1.1 (14)	9.9 (13)	8.7 (13)	$3-10\,(13)$ [2]
	8.1 (13)	8.1 (13)	8.2 (13)	8.8 (13)	9.8 (13)	9.9 (13)	9.4 (13)	8.2 (13)	
C_3H	1.4 (15)	1.2 (15)	8.0 (14)	3.3 (14)	1.5 (14)	8.4 (13)	5.6 (13)	3.8 (13)	
	5.6 (14)	4.1 (14)	2.4 (14)	1.2 (14)	5.7 (13)	3.3 (13)	2.4 (13)	1.5 (13)	2 (14) [8]
	1.3 (13)	1.2 (13)	1.3 (13)	1.6 (13)	1.3 (13)	8.7 (12)	6.0 (12)	4.1 (12)	
C_4H	1.4 (15)	1.1 (15)	5.0 (14)	1.9 (14)	8.9 (13)	5.2 (13)	3.6 (13)	2.4 (13)	
	7.3 (13)	4.7 (13)	3.0 (13)	2.2 (13)	1.7 (13)	1.2 (13)	8.8 (12)	6.1 (12)	$1-4\,(15)$ [4]
	8.5 (12)	8.0 (12)	7.9 (12)	8.9 (12)	1.0 (13)	8.8 (12)	6.4 (12)	4.4 (12)	
C_3H_2	1.9 (13)	1.8 (13)	1.4 (13)	1.0 (13)	7.6 (12)	5.7 (12)	4.2 (12)	3.0 (12)	
	9.8 (12)	8.2 (12)	7.1 (12)	6.4 (12)	5.7 (12)	4.5 (12)	3.4 (12)	2.4 (12)	1 (14) [3]
	3.4 (12)	3.4 (12)	3.5 (12)	4.0 (12)	4.5 (12)	3.9 (12)	2.9 (12)	2.1 (12)	
CH_3OH	2.8 (13)	1.7 (13)	5.2 (12)	1.6 (12)	6.7 (11)	3.7 (11)	2.4 (11)	1.7 (11)	
	2.6 (13)	1.6 (13)	5.8 (12)	1.8 (12)	7.7 (11)	4.2 (11)	2.8 (11)	1.9 (11)	$2-4\,(13)$ [2]
	7.2 (11)	5.2 (11)	2.8 (11)	1.3 (11)	5.5 (10)	3.0 (10)	2.0 (10)	1.4 (10)	
CN	1.3 (14)	1.2 (14)	1.1 (14)	9.5 (13)	8.2 (13)	7.8 (13)	7.5 (13)	6.6 (13)	
	1.6 (14)	1.5 (14)	1.3 (14)	1.0 (14)	8.2 (13)	7.4 (13)	6.9 (13)	5.9 (13)	3 (14) [3]
	8.6 (13)	8.7 (13)	9.3 (14)	1.0 (14)	8.1 (13)	7.2 (13)	6.7 (13)	5.8 (13)	
HCN	3.5 (14)	2.4 (14)	9.7 (13)	4.0 (13)	1.9 (13)	1.0 (13)	7.0 (12)	4.8 (12)	
	3.4 (14)	2.0 (14)	7.5 (13)	3.2 (13)	1.5 (13)	8.4 (12)	5.6 (12)	3.8 (12)	2 (14) [3]
	8.0 (13)	6.4 (13)	3.7 (13)	1.8 (13)	8.9 (12)	5.0 (12)	3.4 (12)	2.3 (12)	
HC_3N	1.0 (14)	5.4 (13)	1.4 (13)	4.4 (12)	1.9 (12)	1.0 (12)	6.9 (11)	4.7 (11)	
	3.8 (13)	1.4 (13)	3.4 (12)	1.1 (12)	4.7 (11)	2.6 (11)	1.8 (11)	1.2 (11)	6 (13) [3]
	3.4 (10)	2.6 (10)	2.5 (10)	3.0 (10)	2.8 (10)	1.9 (10)	1.3 (10)	8.7 (09)	1.7 (14) [5]
CH_3CN	2.6 (13)	1.4 (13)	3.9 (12)	1.2 (12)	5.1 (11)	2.8 (11)	1.8 (11)	1.3 (11)	
	1.9 (13)	1.0 (13)	3.1 (12)	9.9 (11)	4.2 (11)	2.3 (11)	1.6 (11)	1.1 (11)	5 (12) [6]
	1.3 (11)	1.2 (11)	1.0 (11)	6.9 (10)	3.0 (10)	1.6 (10)	1.1 (10)	7.4 (09)	
NH_3	2.9 (13)	2.5 (13)	1.4 (13)	5.3 (12)	2.3 (12)	1.3 (12)	8.5 (11)	5.8 (11)	
	1.9 (14)	1.6 (14)	7.9 (13)	2.7 (13)	1.2 (13)	6.5 (12)	4.3 (12)	3.0 (12)	2 (14) [5]
	6.3 (14)	5.0 (14)	2.5 (14)	8.5 (13)	3.7 (13)	2.0 (13)	1.3 (13)	9.1 (12)	
N_2H^+	3.3 (11)	3.1 (11)	2.2 (11)	1.0 (11)	4.6 (10)	2.6 (10)	1.7 (10)	1.2 (10)	
	2.1 (12)	2.0 (12)	1.4 (12)	5.7 (11)	2.5 (11)	1.4 (11)	9.2 (10)	6.3 (10)	5 (12) [3]
	4.7 (12)	4.6 (12)	3.7 (12)	1.6 (12)	7.0 (11)	3.8 (11)	2.6 (11)	1.8 (11)	1 (13) [7]
CS	8.2 (15)	8.5 (15)	9.5 (15)	7.7 (15)	4.2 (15)	2.6 (15)	1.8 (15)	1.2 (15)	
	7.2 (15)	7.5 (15)	8.4 (15)	6.6 (15)	3.7 (15)	2.2 (15)	1.6 (15)	1.1 (15)	1 (14) [3]
	5.3 (15)	5.5 (15)	6.1 (15)	4.6 (15)	2.8 (15)	1.8 (15)	1.2 (15)	8.5 (14)	
C_2S	8.4 (13)	8.6 (13)	9.5 (13)	9.0 (13)	4.9 (13)	2.9 (13)	1.9 (13)	1.3 (13)	
	1.2 (14)	1.2 (14)	1.4 (14)	1.2 (14)	6.0 (13)	3.4 (13)	2.3 (13)	1.6 (13)	1 (14) [4]
	6.4 (13)	6.5 (13)	6.9 (13)	7.6 (13)	4.4 (13)	2.6 (13)	1.7 (13)	1.2 (13)	
C_3S	1.7 (13)	1.7 (13)	1.8 (13)	1.5 (13)	8.0 (12)	4.5 (12)	3.0 (12)	2.1 (12)	
	1.2 (13)	1.2 (13)	1.3 (13)	1.2 (13)	6.3 (12)	3.6 (12)	2.4 (12)	1.6 (12)	$2 \pm 0.4\,(13)$ [4]
	4.4 (12)	4.4 (12)	4.4 (12)	5.2 (12)	3.5 (12)	2.1 (12)	1.4 (12)	9.4 (11)	
HCS^+	6.4 (11)	6.6 (11)	7.2 (11)	5.9 (11)	4.2 (11)	3.0 (11)	2.3 (11)	1.3 (11)	
	7.6 (11)	7.9 (11)	8.7 (11)	6.4 (11)	4.3 (11)	3.0 (11)	2.3 (11)	1.7 (11)	$1 \pm 0.3\,(13)$ [4]
	7.1 (11)	7.4 (11)	8.2 (11)	5.9 (11)	4.1 (11)	2.9 (11)	2.2 (11)	1.6 (11)	
SO	6.2 (11)	6.2 (11)	6.6 (11)	7.8 (11)	7.1 (11)	5.1 (11)	3.7 (11)	2.6 (11)	
	1.5 (12)	1.6 (12)	1.6 (12)	1.4 (12)	1.0 (12)	6.8 (11)	4.8 (11)	3.4 (11)	5 (13) [3]
	2.5 (14)	2.7 (14)	2.4 (14)	8.4 (13)	3.6 (13)	2.0 (13)	1.4 (13)	9.2 (12)	

[1] Schilke et al. (1995), [2] Pratap et al. (1997), [3] Ohishi et al. (1992), [4] Hirahara et al. (1992)
[5] Suzuki et al. (1992), [6] Minh et al. (1993), [7] Hirahara et al. (1995), [8] Ohishi & Kaifu (1998)

order of magnitude larger than the observed values. Pratap et al. (1997) derived a column density of CS, using $C^{34}S$ and an isotopic ratio of $^{32}S/^{34}S = 14$, in the range $\sim 2\times(10^{13}-10^{14})$ cm^{-2}; the upper limit of this range agrees with the measured value of Ohishi et al. (1992). Even with an isotope ratio of $^{32}S/^{34}S = 22$, used for Galactic star forming regions, the upper limit of measured abundances of CS will still be about an order of magnitude lower than our predicted value. However, although the $^{32}S/^{34}S$ ratio in nearby dark clouds remains uncertain (Pratap et al. 1997), we believe the adopted value of this ratio, on its own, cannot explain the large discrepancy between the predicted CS column density and the observations. In order to understand the CS gas phase chemistry we analysed the results in the standard model. In the intermediate region with

local $A_{\rm v} \sim 4$–6, where sulphur is not greatly depleted and CS is most abundant, during early times $t \lesssim 10^4$ years is,

$$\mathrm{S} \xrightarrow{\mathrm{C}^+} \mathrm{S}^+ \xrightarrow{\mathrm{C_2}} \mathrm{CS}^+ \xrightarrow{\mathrm{H_2}} \mathrm{HCS}^+ \xrightarrow{\mathrm{e}} \mathrm{CS} \qquad \text{(R16)}$$

Then until about 2×10^5 years the production and destruction of CS is locked in the recycling sequence,

$$\mathrm{CS} \xrightarrow{\mathrm{H}^+} \mathrm{CS}^+ \xrightarrow{\mathrm{H_2}} \mathrm{HCS}^+ \xrightarrow{\mathrm{e}} \mathrm{CS} \qquad \text{(R17)}$$

and finally, at times $t \gtrsim 3 \times 10^5$ years, when $\mathrm{H_3^+}$ and $\mathrm{HCO^+}$ are available, CS is recycled through the sequence,

$$\mathrm{CS} \xrightarrow{\mathrm{H_3^+, H^+, HCO^+}} \mathrm{CS}^+ \xrightarrow{\mathrm{H_2}} \mathrm{HCS}^+ \xrightarrow{\mathrm{e}} \mathrm{CS} \qquad \text{(R18)}$$

Therefore, once CS is formed it is not effectively lost in the gas phase; because at early times the CS reaction with $\mathrm{H^+}$ and at later times the reactions with $\mathrm{H_3^+}$ and $\mathrm{HCO^+}$ lead to efficient production of precursor ions $\mathrm{CS^+}$ and $\mathrm{HCS^+}$which are almost entirely converted back to CS. From the centre of the cloud to a lower $A_{\rm v} \sim 4$ mag, where the sulphur is not greatly depleted, at all times $t \gtrsim 10^4$ years the chemistry of CS is almost entirely limited to the reaction sequence (R17).

The chemistry of $\mathrm{HCS^+}$ is also restricted to the same reaction sequences above. Decreasing the electron recombination of $\mathrm{HCS^+}$ and increasing the rate of reaction between CS and $\mathrm{H_3^+}$, as investigated by Millar & Herbst (1990), will increase the abundance of $\mathrm{HCS^+}$, but cannot significantly reduce the predicted CS column density and improve the overall agreement with observations for the abundances of S-bearing species.

The predicted peak column density of $\mathrm{HCS^+}$ in our standard model is $\sim 8 \times 10^{11}\ \mathrm{cm^{-2}}$. This value of the column density occurs at about $t \gtrsim 8 \times 10^5$ years and is about an order of magnitude lower than the measured values in the range of $(5$–$10) \times 10^{12}\ \mathrm{cm^{-2}}$ (Hirahara et al. (1992); Ohishi et al. (1992). The predicted column density of $\mathrm{HCS^+}$ is closely related to the column density of CS and obviously to the assumed sulphur abundance and depletion. We found that using a fixed sulphur abundance, throughout the cloud at all depths, the predicted column density of sulphur-containing species are overall in less agreement with observations compared to the case of adopting a depth dependent sulphur abundance. Furthermore, increasing or decreasing the fixed fractional abundance of sulphur within two orders of magnitude, will not improve the overall agreement with observations. Clearly, our results imply that assuming a simple depth dependent depletion for sulphur abundance produces an improved overall agreement with observed column densities of sulphur-containing species.

Unfortunately the gas phase chemistry of sulphur-containing species is only partially understood and it has been the subject of several studies (Smith et al. 1988; Millar & Herbst 1990 and references therein) with, so far, no significant overall agreement with observations of dark clouds. Our results show that for the sulphur-bearing carbon-chain molecules, whose chemistry is developed mainly in the early stages of the cloud evolution, the agreement with observations is quite satisfactory. The conflict with observations appears to be mainly related to abundances of CS and the sulphur-containing "late type" species; indicating the importance of considering time dependent depletion of sulphur abundance as well as the depth dependent depletion. From our results, it appears that there are fundamental processes related to sulphur chemistry in the late stages of the dark cloud evolution which at present are not accounted for and are probably related to gas/grain interactions. We found that the CO depletion onto grains greatly affects the column density of non-carbon sulphur-containing species (e.g. SO and thus $\mathrm{SO_2}$) at later times. In addition to an improved gas phase chemistry, the role of accretion onto grains and grain surface reactions involving O, N and S-containing species could produce improved results which are in closer agreement with observations of sulphur-containing species.

4.4. CO *and* $\mathrm{HCO^+}$

In the regions of the cloud confined to $2 \lesssim A_{\rm v} \leq 8$ mag, at $t \lesssim 3 \times 10^5$ years, the CO formation is mostly via reactions between atomic oxygen and $\mathrm{CH_2}$, CH and $\mathrm{C_2}$. The electron recombination of $\mathrm{HCO^+}$ becomes the dominant production source of CO after $t \gtrsim 4 \times 10^5$ years. The reactions of O with $\mathrm{C_{3,4,5}}$ and C with $\mathrm{C_2H}$ and CH together contribute to about 10% of the CO production at all times. In the outer regions, where $A_{\rm v} \sim 1$, the reactions of O with CH, $\mathrm{C_2}$ and $\mathrm{CH_2}$ produce $\sim$ 70–80% of CO at all times and $\mathrm{HCO^+}$ recombination produces only a maximum of about 10% of CO. In the inner parts of the cloud the main loss of CO is via reactions with major ions, $\mathrm{H_3^+}$ and $\mathrm{He^+}$. In the lower density cloud envelope, where $A_{\rm v} \lesssim 2$ mag, the loss of CO is dominated by UV photodissociation at all times.

Column densities of CO toward dark cloud cores have been derived in several studies using mainly rarer isotopic variations like $\mathrm{C^{18}O}$ and assuming $^{16}\mathrm{O}/^{18}\mathrm{O} \sim 500$, or ^{13}CO and assuming $^{12}\mathrm{C}/^{13}\mathrm{C} = 64$ (Pratap et al. 1997), or assuming a terrestrial value for $^{12}\mathrm{C}/^{13}\mathrm{C}$ ratio of 89 (McCutcheon et al. 1980). The derived observed column density of CO for several dark clouds reported by Irvine et al. (1987) is $8 \times 10^{17}\ \mathrm{cm^{-2}}$ which is in the middle of the range of $(4$–$12) \times 10^{17}\ \mathrm{cm^{-2}}$ found by Pratap et al. (1997) and Schilke et al. (1995) for TMC-1. In our standard model the predicted equilibrium value of the CO column density, reached at about 5×10^6 years, is $3 \times 10^{17}\ \mathrm{cm^{-2}}$. As shown in Table 2, our predicted column density of CO is in good agreement with observations. Several observations reported abundances (relative to molecular hydrogen) of CO toward dark clouds; fractional abundances ranging between 4–10×10^{-5} are derived in various observations, using a total hydrogen column density of $10^{22}\ \mathrm{cm^{-2}}$ (Ohishi et al. 1992; Pratap et al. 1997). The calculated CO abundances, for various depth, listed in Table 3 are in good agreement with observations of dark clouds.

It is important to emphasize the critical role of CO depletion and desorption processes in improving the predicted column density of CO to a level where a good agreement with observations is achieved. Our results show that in the absence of CO accretion, the column density of CO in the gas phase reaches an equilibrium value of about $5 \times 10^{18}\ \mathrm{cm^{-2}}$, (equivalent to an abundance of 3.72×10^{-4} at the centre of the cloud) thus

Table 3. Local abundances (relative to hydrogen) of selected species for various distances r (in pc) from the cloud centre and evolution times (2×10^5, 5×10^5 and 1×10^6 years) in the standard model; the total cloud radius is $R = 0.64$ pc and $A_v(r)$ is the local A_v at a radial depth $R - r$ from the cloud surface. The quoted observed abundances are derived from observed column densities by dividing with a total hydrogen number density $N_H = 1 \times 10^{22} cm^{-2}$. Note: $x(y)$ refers to $x \times 10^y$.

r [pc]	0.00	0.02	0.03	0.05	0.07	0.10	0.13	0.20	TMC-1
A_v(r) [mags]	8.0	6.9	6.2	5.2	4.7	3.6	2.8	1.8	
	9.6 (-05)	1.0 (-04)	1.1 (-04)	1.3 (-04)	1.6 (-04)	2.4 (-04)	3.2 (-04)	3.2 (-04)	
C	4.1 (-06)	5.5 (-06)	8.9 (-06)	1.8 (-05)	4.1 (-05)	1.6 (-04)	2.9 (-04)	3.1 (-04)	$1 - 10$ (-05) [1]
	5.9 (-09)	1.5 (-08)	3.5 (-08)	1.4 (-07)	1.2 (-06)	9.4 (-05)	2.6 (-04)	3.1 (-04)	
	1.4 (-04)	1.4 (-04)	1.4 (-04)	1.4 (-04)	1.3 (-04)	8.9 (-05)	3.7 (-05)	8.3 (-06)	
CO	6.8 (-05)	7.1 (-05)	7.6 (-05)	8.6 (-05)	9.5 (-05)	7.7 (-05)	3.4 (-05)	7.5 (-06)	$8 - 12$ (-05) [2]
	1.5 (-05)	1.6 (-05)	1.7 (-05)	2.1 (-05)	3.1 (-05)	5.3 (-05)	3.0 (-05)	7.3 (-06)	
	1.5 (-07)	7.6 (-08)	4.4 (-08)	2.2 (-08)	1.1 (-08)	1.7 (-09)	4.0 (-10)	3.3 (-11)	
H_2CO	1.0 (-07)	4.1 (-08)	2.7 (-08)	1.9 (-08)	1.0 (-08)	1.8 (-09)	4.2 (-10)	3.3 (-11)	5 (-08) [8]
	3.7 (-09)	1.3 (-09)	9.4 (-10)	9.3 (-10)	1.4 (-09)	1.7 (-09)	4.4 (-10)	3.3 (-11)	
	5.0 (-10)	4.6 (-10)	4.2 (-10)	3.4 (-10)	2.2 (-10)	5.6 (-11)	2.6 (-11)	9.0 (-12)	
HCO^+	4.6 (-10)	4.9 (-10)	5.1 (-10)	4.9 (-10)	2.9 (-10)	5.6 (-11)	2.5 (-11)	8.4 (-12)	$2 - 4$ (-09) [2]
	1.6 (-10)	1.7 (-10)	1.9 (-10)	2.3 (-10)	2.2 (-10)	5.0 (-11)	2.6 (-11)	8.3 (-12)	
	6.5 (-09)	7.2 (-09)	8.0 (-09)	9.4 (-09)	1.2 (-08)	1.8 (-08)	3.2 (-08)	1.0 (-07)	
CH	6.0 (-10)	6.5 (-10)	1.0 (-09)	2.1 (-09)	4.7 (-09)	1.5 (-08)	3.1 (-08)	9.5 (-08)	2 (-08) [3]
	1.1 (-11)	8.2 (-12)	1.2 (-11)	3.6 (-11)	2.2 (-10)	1.0 (-08)	2.9 (-08)	9.4 (-08)	
	2.3 (-09)	2.2 (-09)	2.3 (-09)	2.6 (-09)	3.1 (-09)	3.4 (-09)	4.9 (-09)	1.3 (-08)	
C_2H	7.4 (-10)	3.2 (-10)	3.3 (-10)	5.8 (-10)	1.0 (-09)	2.4 (-09)	4.5 (-09)	1.2 (-08)	$3 - 10$ (-09) [2]
	5.9 (-12)	4.1 (-12)	5.5 (-12)	1.6 (-11)	6.6 (-11)	1.3 (-09)	4.1 (-09)	1.1 (-08)	
	1.9 (-07)	1.5 (-07)	1.1 (-07)	7.8 (-08)	4.3 (-08)	6.2 (-09)	2.0 (-09)	4.4 (-10)	
C_3H	1.7 (-07)	4.8 (-08)	2.9 (-08)	2.1 (-08)	1.4 (-08)	4.2 (-09)	1.8 (-09)	4.0 (-10)	2 (-08) [8]
	4.9 (-10)	8.8 (-11)	2.7 (-11)	1.2 (-11)	5.7 (-11)	2.0 (-09)	1.7 (-09)	4.0 (-10)	
	4.1 (-07)	1.5 (-07)	8.2 (-08)	4.0 (-08)	1.7 (-08)	2.2 (-09)	1.5 (-09)	1.2 (-09)	
C_4H	3.0 (-08)	4.3 (-09)	2.1 (-09)	1.6 (-09)	1.6 (-09)	1.0 (-09)	1.3 (-09)	1.1 (-09)	$1 - 4$ (-07) [4]
	5.6 (-10)	6.8 (-11)	1.1 (-11)	9.7 (-13)	1.0 (-12)	2.7 (-10)	1.1 (-09)	1.1 (-09)	
	1.9 (-09)	1.4 (-09)	1.2 (-09)	9.2 (-10)	7.6 (-10)	4.6 (-10)	5.1 (-10)	5.4 (-10)	
C_3H_2	1.7 (-09)	4.2 (-10)	2.6 (-10)	2.5 (-10)	3.0 (-10)	3.2 (-10)	4.7 (-10)	4.9 (-10)	1 (-08) [3]
	1.9 (-11)	2.6 (-12)	1.5 (-12)	1.8 (-12)	5.8 (-12)	1.6 (-10)	4.2 (-10)	4.9 (-10)	
	1.0 (-08)	2.8 (-09)	9.4 (-10)	2.3 (-10)	5.2 (-11)	2.4 (-12)	1.4 (-13)	9.1 (-16)	
CH_3OH	1.0 (-08)	2.6 (-09)	1.1 (-09)	3.4 (-10)	8.5 (-11)	2.9 (-12)	1.5 (-13)	9.0 (-16)	$2 - 4$ (-09) [2]
	2.1 (-10)	7.0 (-11)	3.8 (-11)	2.0 (-11)	1.4 (-11)	3.4 (-12)	1.7 (-13)	9.1 (-16)	
	5.9 (-09)	5.7 (-09)	5.2 (-09)	4.7 (-09)	4.1 (-09)	3.2 (-09)	2.9 (-09)	7.1 (-09)	
CN	1.4 (-08)	9.1 (-09)	8.0 (-09)	7.1 (-09)	6.0 (-09)	3.9 (-09)	3.0 (-09)	6.5 (-09)	3 (-08) [3]
	1.6 (-10)	2.9 (-10)	5.6 (-10)	1.3 (-09)	3.8 (-09)	5.6 (-09)	3.1 (-09)	6.4 (-09)	
	1.1 (-07)	3.6 (-08)	1.5 (-08)	6.1 (-09)	3.3 (-09)	1.4 (-09)	3.4 (-10)	4.6 (-11)	
HCN	1.4 (-07)	2.9 (-08)	1.0 (-08)	4.2 (-09)	2.6 (-09)	1.2 (-09)	3.1 (-10)	4.1 (-11)	2 (-08) [3]
	1.8 (-08)	8.0 (-09)	5.2 (-09)	3.0 (-09)	1.6 (-09)	9.4 (-10)	3.1 (-10)	4.0 (-11)	
	4.7 (-08)	8.9 (-09)	2.3 (-09)	4.6 (-10)	1.2 (-10)	1.5 (-11)	5.3 (-12)	9.7 (-13)	
HC_3N	2.6 (-08)	2.0 (-09)	4.1 (-10)	9.1 (-11)	3.1 (-11)	8.4 (-12)	4.6 (-12)	8.9 (-13)	6 (-09) [3]
	1.4 (-11)	3.6 (-13)	1.2 (-13)	1.1 (-13)	2.6 (-13)	2.7 (-12)	4.0 (-12)	8.8 (-13)	1.7 (-08) [5]
	1.2 (-08)	2.3 (-09)	6.2 (-10)	1.4 (-10)	3.9 (-11)	2.9 (-12)	1.4 (-13)	1.9 (-15)	
CH_3CN	9.3 (-09)	1.6 (-09)	4.9 (-10)	1.6 (-10)	5.6 (-11)	3.2 (-12)	1.3 (-13)	1.7 (-15)	5 (-10) [6]
	1.7 (-11)	7.6 (-12)	7.6 (-12)	8.4 (-12)	9.3 (-12)	3.3 (-12)	1.4 (-13)	1.6 (-15)	
	5.7 (-09)	3.3 (-09)	2.2 (-09)	1.2 (-09)	5.7 (-10)	9.1 (-11)	1.8 (-11)	4.1 (-13)	
NH_3	3.7 (-08)	2.4 (-08)	1.4 (-08)	6.5 (-09)	2.4 (-09)	2.3 (-10)	3.3 (-11)	3.9 (-13)	2 (-08) [5]
	1.4 (-07)	7.4 (-08)	4.3 (-08)	2.0 (-08)	8.1 (-09)	5.2 (-10)	4.8 (-11)	4.0 (-13)	
	3.5 (-11)	3.3 (-11)	2.9 (-11)	2.2 (-11)	1.3 (-12)	3.0 (-12)	8.4 (-13)	8.6 (-14)	
N_2H^+	2.1 (-10)	2.1 (-10)	2.0 (-10)	1.6 (-10)	7.7 (-11)	9.0 (-12)	1.6 (-12)	8.2 (-14)	5 (-10) [3]
	4.0 (-10)	4.1 (-10)	4.2 (-10)	4.2 (-10)	2.9 (-10)	2.2 (-11)	2.4 (-12)	8.2 (-14)	1 (-09) [7]
	3.1 (-08)	1.5 (-07)	3.4 (-07)	6.5 (-07)	9.2 (-07)	5.6 (-07)	2.1 (-07)	8.1 (-08)	
CS	2.9 (-08)	1.4 (-07)	3.2 (-07)	6.0 (-07)	8.0 (-07)	4.6 (-07)	2.0 (-07)	7.4 (-08)	1 (-08) [3]
	2.3 (-08)	1.2 (-07)	2.7 (-07)	4.9 (-07)	5.2 (-07)	3.3 (-07)	1.9 (-07)	7.3 (-08)	
	4.5 (-10)	1.3 (-09)	2.1 (-09)	4.1 (-09)	8.8 (-09)	8.9 (-09)	2.4 (-09)	4.7 (-10)	
C_2S	7.0 (-10)	2.1 (-09)	4.0 (-09)	8.1 (-09)	1.5 (-08)	9.5 (-09)	2.4 (-09)	4.3 (-10)	1 (-08) [4]
	4.7 (-10)	9.8 (-10)	1.3 (-09)	1.6 (-09)	3.5 (-09)	9.9 (-09)	2.4 (-09)	4.3 (-10)	
	2.2 (-10)	4.8 (-10)	6.7 (-10)	1.9 (-09)	1.8 (-09)	1.3 (-09)	3.4 (-10)	3.6 (-11)	
C_3S	1.9 (-10)	2.9 (-10)	3.7 (-10)	6.0 (-10)	1.2 (-09)	1.1 (-09)	3.3 (-10)	3.3 (-11)	2 ± 0.4 (-09) [4]
	8.8 (-11)	9.3 (-11)	7.1 (-11)	4.4 (-11)	9.0 (-11)	7.9 (-10)	3.1 (-10)	3.3 (-11)	
	1.8 (-12)	1.0 (-11)	2.6 (-11)	4.7 (-11)	5.2 (-11)	3.7 (-11)	2.9 (-11)	2.1 (-11)	
HCS^+	2.5 (-12)	1.4 (-11)	3.6 (-11)	7.1 (-11)	6.9 (-11)	3.6 (-11)	3.0 (-11)	1.9 (-11)	1 ± 0.3 (-09) [4]
	2.3 (-12)	1.3 (-11)	3.3 (-11)	7.1 (-11)	6.9 (-11)	3.1 (-11)	3.0 (-11)	1.9 (-11)	
	1.1 (-13)	5.2 (-13)	1.2 (-12)	3.6 (-12)	1.3 (-11)	6.8 (-11)	7.9 (-11)	4.1 (-11)	
SO	1.2 (-11)	4.4 (-11)	6.3 (-11)	8.0 (-11)	1.1 (-10)	1.1 (-10)	8.6 (-11)	4.0 (-11)	5 (-09) [3]
	4.0 (-09)	2.0 (-08)	3.4 (-08)	3.2 (-08)	1.1 (-08)	2.2 (-10)	9.7 (-11)	4.0 (-11)	

[1] Schilke et al. (1995), [2] Pratap et al. (1997), [3] Ohishi et al. (1992), [4] Hirahara et al. (1992)
[5] Suzuki et al. (1992), [6] Minh et al. (1993), [7] Hirahara et al. (1995), [8] Ohishi & Kaifu (1998)

carrying over 99% of the total C at times $t \gtrsim$ a few$\times 10^5$ years. This implies that virtually all carbon in the core of the cloud is in CO after about half a million years – a result which is not in accordance with observations (see the discussion on CO depletion onto grains in Sect. 4.7). The present results confirm that the CO and HCO^+ chemistry are closely linked, similar to the connected chemistry of NH_3 and N_2H^+ (see Sect. 4.5). Furthermore, there is an obvious anti-correlation between CO and NH_3 at times $t \gtrsim 5 \times 10^5$ years when CO depletion becomes significant. We found that with increasing CO depletion the abundance of NH_3 increases (by a factor of 10–15), resulting in much closer agreement with observations for both NH_3 and N_2H^+ (see Sects. 4.5 and 4.7 for explanation).

In Figs. 3a to 3f, the distributions of CO, HCO^+, NH_3 and N_2H^+ are displayed in various forms: (a) fractional abundances at the centre of the cloud, (b) variation of fractional abundances with radius corresponding to the central line of sight at $t = 10^6$ years, (c) time variation of column densities along the central line of sight, (d) a comparison between the column densities of CO, NH_3 and HC_3N along the central line of sight and the corresponding average column densities using a beam radius of 0.1 pc, (e) the effects of grain accretion and desorption (by cosmic-ray spot heating) on the abundance of CO and finally (f) same as (e) but showing the effects on the column density of CO. In Figs. 4b, 4c and 4d the radial distribution of CO as a function of A_v is displayed for several cases. As shown in Figs. 3e, 4c and 4d, the equilibrium abundance of CO in our standard model can be increased by assuming a smaller sticking coefficient or assuming larger grain sizes and therefore smaller accretion rates. In addition, the rate of desorption can be increased by considering combined effects of other possible desorption processes, e.g. cosmic-ray-induced desorption. Improved assumptions related to the size and surface properties of grains varying with time and local conditions will allow a better understanding of the chemistry and properties of the cloud evolution at later times.

The production of HCO^+ at higher density ($A_v \gtrsim 3$ mag) is largely via reaction of CO and H_3^+, atomic O and CH_3^+, C^+ and H_2O, and the exchange reaction between O and CH, where reactions involving C^+ and O contribute more at earlier times while the production involving H_3^+ becomes dominant after $t \sim 10^5$ years. Similar reactions control the production of HCO^+ in all moderate depths until about an $A_v \lesssim 2$ mag when the exchange reaction of O with CH becomes dominant over the production via CO and H_3^+. The loss of HCO^+ at all densities and times is largely by dissociative recombination with electrons. The distribution and extent of HCO^+ follows closely that of CO in all models. Our predicted peak column density of HCO^+ in the standard model is 6×10^{12} cm^{-2}, approximately a factor of 10 lower than the measured column densities, $(5\text{–}10) \times 10^{13}$ cm^{-2}, which have been derived assuming various abundance ratios of $^{12}C/^{13}C = 45$–90 (Turner 1994; Pratap et al. 1997). Our predicted HCO^+ column density can be improved by at least a factor of 5 in the case of assuming a low metal abundance (e.g. assuming a metal abundance of $\sim 10^{-8}$ produces a peak column density of 2.3×10^{13} cm^{-2}). The HCO^+ column density can also be improved to match the observed value by assuming a higher cosmic-ray ionization rate (e.g. $\zeta_{cr} = 5 \times 10^{-17}$ s^{-1}, produces a peak column density of $\sim 10^{13}$ cm^{-2}). It should be noted that the low predicted abundance of HCO^+ is not related to the CO depletion from the gas phase; our results show that the abundance of HCO^+ is at most 50% higher in the absence of CO accretion. Clearly, the chemistry of HCO^+ and CO needs to be studied in greater depth; including a detailed treatment of CO photodissociation and the related grain surface chemistry will probably lead to a better understanding of the overall chemistry and cloud chemical evolution.

4.5. NH_3 *and* N_2H^+

The formation of NH_3 for $A_v \sim 2$–8 mag is dominated by the reaction sequence,

$$N_2 \xrightarrow{He^+} N^+ \xrightarrow{H_2} NH^+ \xrightarrow{H_2} NH_2^+ \xrightarrow{H_2} NH_3^+ \xrightarrow{H_2} NH_4^+ \xrightarrow{e} NH_3 \quad \text{(R19)}$$

In reaction sequence (R19) the production of the parent molecule, N_2, varies with cloud depth; at $t \gtrsim 10^4$ years and moderate $A_v \sim 2$–3 mag, N_2 is formed via reaction chain,

$$C_2H_2^+ \xrightarrow{e} C_2 \xrightarrow{N} CN \xrightarrow{N} N_2 \quad \text{(R20)}$$

where $C_2H_2^+$ is formed through a series of reactions beginning with C^+ reacting with CH, followed by H-atom abstraction reactions of hydrocarbon ions; at higher $A_v \sim 3$–8 mag, when cosmic-ray ionization is effective, the formation of N_2 is mainly via,

$$O \xrightarrow{H_3^+} OH^+ \xrightarrow{H_2} H_2O^+ \xrightarrow{H_2} H_3O^+ \xrightarrow{e} OH \xrightarrow{N} NO \xrightarrow{C} CN \xrightarrow{N} N_2 \quad \text{(R21)}$$

at times $t \gtrsim 10^4$ years. In addition, towards the centre of the cloud for $t \gtrsim 5 \times 10^5$ years, the following sequence,

$$N_2 \xrightarrow{H_3^+} N_2H^+ \xrightarrow{e} N_2 \quad \text{(R22)}$$

continuously recycles N_2.

At earlier times and for densities ~ 1–3×10^3 cm^{-3} (equivalent to $\sim A_v \lesssim 2$ mag) the H-atom abstraction reaction of N_2^+ is by large the main production source of N_2H^+, but further inside the cloud the reaction of N_2 and H_3^+ is responsible for the observed abundance of N_2H^+. Therefore, N_2 appears to be the parent species for the production of both NH_3 (through reaction with He^+) and N_2H^+ (through reaction with H_3^+); thus probably explaining the observed connection between NH_3 and N_2H^+ (Hirahara et al. 1995).

At later times $t \gtrsim 5 \times 10^5$ years, as more H_3^+ becomes available due to loss of CO from the gas phase, NH_3 is more efficiently produced - i.e. in the region where the extinction or the grain density is high. Ammonia is not easily destroyed because the main loss of NH_3 (about 80%) is by reactions with abundant ions, C^+, H_3^+, H_3O^+ and HCO^+ resulting in the formation of NH_3^+ and NH_4^+ which rapidly recombine to form NH_3. At all times, only a total of about 20% of NH_3 is effectively lost from the system by reaction with CN (and subsequent production of HNC) and reaction with C^+ (and subsequent production of H_2NC^+ leading to formation of HNC and CN).

NH_3 is one of the most observed molecules toward dark cloud cores and small clumps including TMC-1. The observed column density of NH_3 in these cores is given in the range of $(4\text{–}14) \times 10^{14}$ cm^{-2} (Benson & Myers 1989; Suzuki et al. 1992; Hirahara et al. 1992). In our standard model, the predicted maximum column density of ammonia for the central line of sight is 7×10^{14} cm^{-2} which it is obtained at about 5×10^6 years (Fig. 3c). The peak column density of ammonia once reached

remains unchanged for the remaining period of the cloud evolution. Increasing the cloud density up to about 10^5 cm^{-3} does not appear to have a substantial effect in increasing the column density of NH_3. However, increasing the visual extinction, at the centre of the cloud, from $(A_v)_c = 8$ to 10 mag, increases the calculated peak column density in the standard model to about 2×10^{15} cm^{-2} which agrees with the upper limit of the present measured values, indicating that the upper limit of the observed column density of NH_3 is probably associated with cores with a higher optical depth. In addition, increasing the cosmic-ray ionization rate ζ_{cr} to 5×10^{-17} s^{-1} in the standard model increases the peak column density of NH_3 to about 9.5×10^{14} cm^{-2} which is closer to the average of measured values.

The observed column density of N_2H^+ is given in the range of $(1–5) \times 10^{12}$ cm^{-2} by Pratap et al. (1997) and Ohishi et al. (1992), which is about a factor of two smaller than the column density of $(1–1.5) \times 10^{13}$ cm^{-2} derived by Hirahara et al. (1995). Our predicted maximum column density of N_2H^+ is 5.5×10^{12} cm^{-2} at the peak column density of ammonia. Similar to NH_3, with higher core extinction or higher cosmic-ray ionization rate and/or higher CO accretion rate, the predicted column density of N_2H^+ increases to $\sim 10^{13}$ cm^{-2}, in good agreement with the upper limit of the observed values.

4.6. The effects of cosmic-ray-induced photons

The cosmic-ray-induced ultraviolet photons provide an internal source of radiation in dense clouds; they are formed most efficiently by impact excitation of molecular hydrogen from secondary electrons generated by cosmic-ray ionization of H_2 (Prasad & Tarafdar 1983). Since in dense molecular cores hydrogen is almost entirely in molecular form, the cosmic-ray-induced photoionization/dissociation is expected to be most effective. In our standard model we have adopted the CRI photodissociation and photoionization rates from Gredel et al. (1989), assuming a $\zeta_{cr} = 3 \times 10^{-17}$ s^{-1} and a grain albedo $\omega = 0.3$; for CO we allowed a CRI photodissociation rate which is temperature dependent (Gredel et al. 1987; Rawlings et al. 1992).

Cosmic-ray-induced photoionization and photodissociation reactions have significant effects on the predicted abundances of several species, particularly, HCN, HC_3N, C_2S, CH_3CN, CH_3OH, C_6H and CH_4. It appears that, generally most critically affected species are the "early type" species which reach their maximum abundances by early times of $\sim$ 3–4$\times 10^5$ years, mainly because of a substantial increase in the abundance of C^+. Moreover, by considering the chemical evolution of HC_3N, C_2S and CH_3CN above, both with respect to time and depth, it emerges that the standard model and Model A (no CRI photons) mainly differ in the degree of fractional ionization which is higher in the standard model due to internally generated CRI photons. Figs. 5a, 5b and 5c display for both models the time variation of the electron abundance calculated at various depth positions: at the centre of the cloud ($A_v = 8$ mag) and at positions where $A_v \sim 4$ mag and $A_v \sim 3$ mag, respectively. The effects of additional photons generated by cosmic-rays are most significant at early times up to about few$\times 10^5$ years. With decreasing visual extinction the effects of cosmic-rays-induced photons also becomes less important. Figs. 5d, 5e and 5f show the radial variation of the electron abundance for the standard model and Model A at three different evolution times: $t = 10^4$, $t = 10^5$ and $t = 10^6$ years, respectively. Similar results are apparent - the contribution of cosmic-ray-induced photons to the total electron abundance, and thus the overall chemistry, is most effective at early times up to a few$\times 10^5$ years and up to a radius of about 0.2 pc (equivalent to a local $A_v \sim 2$ mag). These results show clearly that it is essential to include the effects of CRI photoionisation/dissociation in models of dense cores. Furthermore, the sensitivity of CH_3CN and C_2S abundances, in particular, to the effects of cosmic-ray-induced photons may be used to measure the cosmic-ray flux in dense molecular cores.

4.7. The effects of the CO depletion onto grains

In order to examine the effects of gas phase depletion onto grains, in this study we only included CO accretion and desorption by direct cosmic ray spot heating. According to Léger et al. (1985), since the binding energy of atoms (O,C,N,...) is about half of that of CO, on a non-reactive surface they would evaporate at temperatures > 10 K; however, before evaporating they can enter into chemical reactions if the number of active sites per unit surface is large enough and/or the activation energies of the reactions are small enough. With atomic O being such a reactive species, it seems necessary to consider the accretion of atomic O with related surface chemistry and desorption mechanism(s) which allow for the return of the gas phase oxygen in some appropriate form. Similarly, consideration of accretion for atomic N and S (or other abundant N and S-bearing species) also requires detailed study of the related surface chemistry and appropriate desorption mechanisms. Moreover, a simple calculation indicates that, since CO and atomic C are approximately some 2–4 orders of magnitude more abundant than hydrocarbons, the timescale for the effective accretion of hydrocarbons will be at least of the order of 10 million years. Hence, the accretion of hydrocarbons probably makes no significant difference in the chemistry of quiescent low mass dark molecular cores, particularly when accretion of CO and atomic C is also included. Therefore, although greatly simplified, in order to study the effects of gas phase depletion onto grains, we only considered CO accretion and desorption by direct cosmic-ray spot heating which has been shown to be effective in the case of CO mantles (Léger et al. 1985). Furthermore, it should be noted that, for a detailed study of the chemical evolution the effects of grain surface chemistry need to be considered; however, it seems more appropriate to investigate these effects in a separate study.

With the CO accretion we found an interesting connection between the variation of NH_3 and CO at times corresponding to the accretion timescale of $t >$ few$\times 10^5$ years. We found that in pure gas phase models the column density of NH_3 reaches at most a value of few$\times 10^{13}$ cm^{-2}, more than a factor of 10 below average measured values for dense cores. In order to understand,

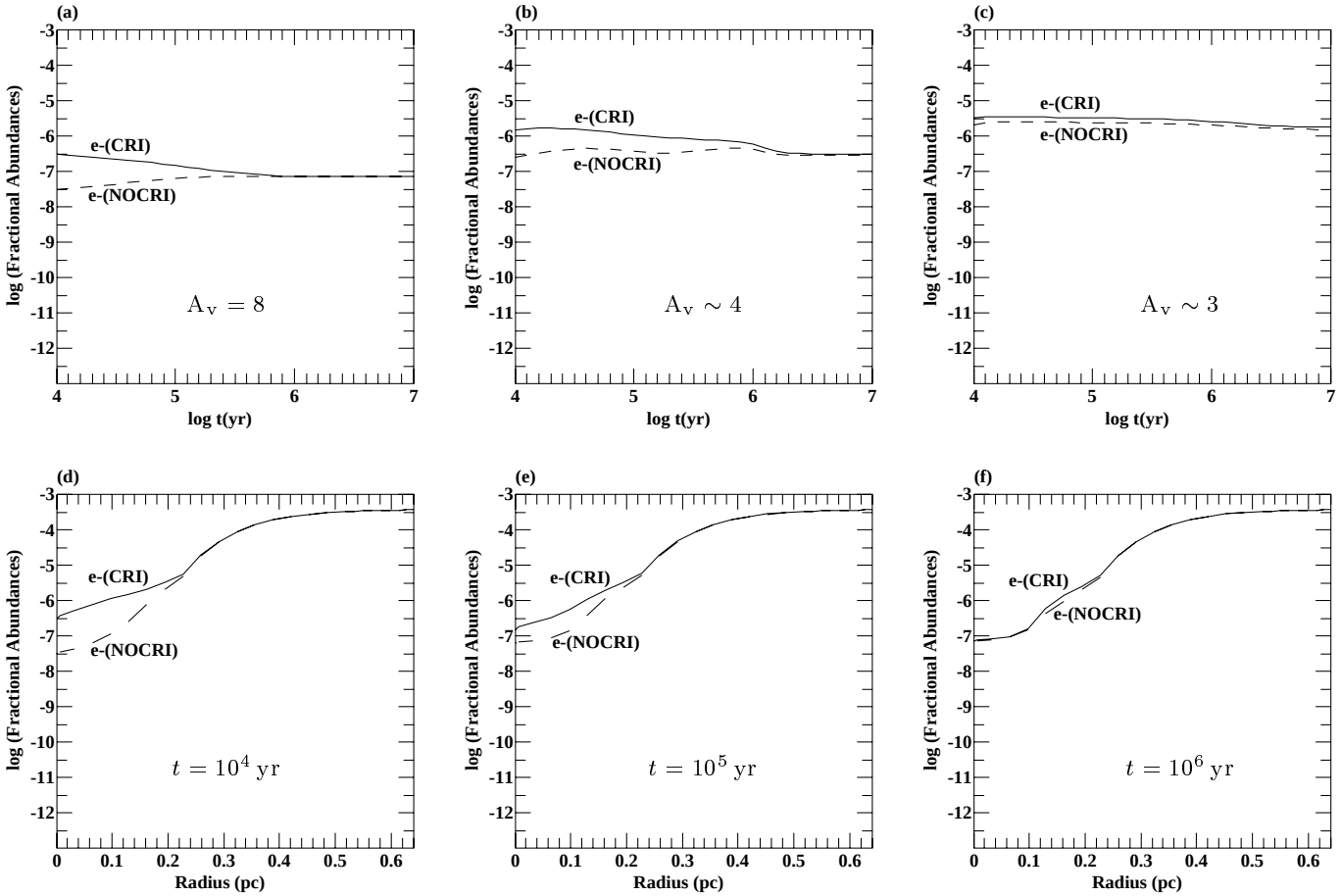

Fig. 5. a Time variation of electron abundances in the standard model (solid line) and in the absence CRI photons (dash line) at the centre of the cloud with an $A_{\rm v} = 8$ mag. **b** As in **a**, but for a depth position with an $A_{\rm v} \sim 4$ mag. **c** As in **a**, but for a depth position with an $A_{\rm v} \sim 3$ mag. **d** Variation of electron abundances in the standard model with radius at a time $t = 10^4$ years. **e** As in **d**, but for the time $t = 10^5$ years. **f** As in **d**, but for the time $t = 10^6$ years.

in detail, the chemical reason(s) for the connection between CO depletion and the increase in the NH_3 abundance, we have analyzed the chemistry for two cases: standard model with CO depletion and Model B without CO depletion using the results corresponding to the centre of the cloud, with highest $A_{\rm v}$ where gas phase accretion onto grains is expected to be most effective. A comparison of abundances between the two models indicates that CO accretion generally affects the overall chemistry by decreasing the abundances of carbon and oxygen containing species. However, the group of species whose maximum abundances are reached at the so-called "early times" are not greatly affected by CO depletion. The "late type" species whose maximum abundances are reached at later times of $\gtrsim 10^6$ years are mostly affected by the loss of CO from the gas phase. A comparison between the two models further shows that the electron abundance is about a factor of 2 lower in the standard model with CO depletion; this is due to a large decrease in the abundance of C^+, in particular, and also a drop in abundances of hydrocarbon ions. However, during the peak-time of CO accretion onto grains, at $t \gtrsim 8 \times 10^5$ years, a dramatic increase by about a factor of 5–10 in the abundances of several species, namely NO, OH, O_2, HS and SO becomes apparent. The increase in abundances of oxygen and sulphur non-carbon-containing molecules is mainly due to the decrease of the gas phase CO abundance which allows more H_3^+ ions to become available for reactions with abundant oxygen, nitrogen and sulphur-bearing species. This condition is exacerbated also by the fact that with the loss of CO from the gas phase there is less C available for reaction with H_3^+; this improves the production of other major ions involving H_3^+, e.g. H_3O^+ (via, $O \xrightarrow{H_3^+} OH^+ \xrightarrow{H_2} H_2O^+ \xrightarrow{H_2} H_3O^+$) and N_2H^+ (because of an increase in production by reaction between H_3^+ and N_2). The enhanced production of NH_3, with the CO accretion onto grains, is largely due to an increase in production of N_2 through an increase in the H_3^+ abundance and the reaction sequence (R19). The close relation between CO depletion and the increase in abundances and column densities of NH_3 and N_2H^+ is displayed in Figs. 3a and 3c. Note that the HCO^+ distribution closely follows that of CO, and N_2H^+ similarly varies with NH_3. The CO depletion also produces an increase (by a factor of 3) in the predicted column densities of OH and H_2O.

Special reference must be made to SO and SO_2 abundances which are most drastically increased by some 2 orders of magnitude at later times under the influence of CO depletion. The peak abundances of SO and SO_2 are attained at later times of $t \gtrsim 10^6$ years and they can therefore be classed as "late type" species. Abundances of all late type species are critically affected by grain related processes in denser part of the cloud. Although there are uncertainties in the chemistry of sulphur-containing species, the results clearly indicate that the CO depletion onto grains has a strong influence on increasing abundances of SO and SO_2 at later times. This increase is due to a more efficient production of parent ions and a decrease in the C/O abundance ratio – less carbon in the gas phase allows more oxygen to become available for reactions with non-carbon-containing species, e.g. via reactions O+HS $\rightarrow$ SO, S+OH $\rightarrow$ SO, O_2+S $\rightarrow$ SO and O+SO $\rightarrow$ SO_2, OH+SO $\rightarrow$ SO_2; the formation of O_2 is, due to an enhanced production of H_3O^+, more efficient with less CO (and thus HCO^+) in the system.

It is worth to note that a similar rise in abundances of sulphur-containing "late type" species or an increase in abundances of NH_3 cannot be simply achieved by adopting a larger C/O abundance ratio for the chemical models, at least without the expenses of losing agreement for some other molecules. The apparent correlation between the abundances of SO and N_2H^+ with NH_3 at later times of the cloud evolution, appears to be closely connected to the effects of the lower CO abundance (and consequently the change in the C/CO abundance ratio and the increase in abundances of non-carbon-containing ions). Our results are consistent with the observations of Ohishi et al. (1992) and those reported by Hirahara et al. (1995) from the measurements of the spatial distributions of SO and N_2H^+ toward TMC-1; they found that the distributions of SO and N_2H^+ are well correlated with those NH_3 and HCO^+. Because of the extreme sensitivity of SO to the CO accretion, we list in Table 4 the calculated column densities for the case of a lower CO sticking coefficient of 0.1; Table 5 lists the corresponding abundances for selected species. Table 4 shows a good overall agreement with observations for the column densities of "early type" as well as the "late type" species. However, the SO abundance can be further modified by adopting a time dependent sulphur depletion and a stronger (direct) oxygen depletion which seems a reasonable assumption considering the high abundances of (non-carbon) oxygen and sulphur containing species. The detection of gas phase H_2O and O_2 in low mass dense clouds will be of potential importance as a diagnostic probe of gas and grain chemistry involving oxygen. Because of the close connection between oxygen and sulphur chemistry and underlying uncertainties related both to gas phase reactions and gas-grain interactions, considerations of depletion and surface chemistry of these species need a more thorough investigation in a separate study.

4.8. The effects of an anisotropic radiation field

In our standard model it is assumed that the cloud is exposed to an isotropic radiation field. Table 6 lists the predicted column densities for the standard model but with a modified external UV radiation field; in this case we assume that the cloud is exposed to a radiation field from a single direction, i.e. the direction of the observer. We have considered this case to demonstrate, in a simple way, the effects of an anisotropic radiation field, e.g. a cloud is exposed to the UV field generated by a nearby star. The main effect on abundances is due to a change in the local A_v, which is higher for the anisotropic case, because the UV photons have to travel a longer way into the cloud compared to the isotropic case where the distance is shortest; a longer distance implies a higher local A_v enhanced by the density gradient inside the cloud. Note that for the central line of sight there is no difference between the two cases because the direction of the line of sight coincides with the direction of the radiation field. The larger the offset of a line of sight from the centre of the cloud, the larger will be the effect of the anisotropic radiation field on the abundances because the UV extinction at a given point will be higher. Therefore, it is expected that species whose abundances are sensitive to A_v and/or density are most effected by an anisotropic radiation field. It should also be noted that in the anisotropic case the total number of external UV photons penetrating the cloud per second is only half of that in the isotropic case.

Table 6 shows the predicted column densities of selected species for various beam sizes. Obviously, the larger the beam size the larger will be the effect of the anisotropic radiation field on the predicted column densities. The column density of species like HC_3N and CH_3CN are most affected because their chemistry is sensitive to UV photons and they are concentrated in the core of the cloud where the density is highest.

5. Concluding remarks

We have studied chemical and physical conditions of dense molecular cores assuming hydrostatic equilibrium and using time dependent spherical polytropic models. As was noted for diffuse cloud applications by van Dishoeck & Black (1986), the polytropic models, although convenient, may not provide realistic temperature and density gradients in the outer part of the cloud. Likewise we have found that the density structure close to the outer boundary cannot be satisfactorily resolved. The characteristic steep density gradient close to the cloud surface is inherent to the polytropic approximation, however this does not have any significant influence on the predicted chemical abundances of dense cloud cores. We found that predicted abundances and column densities for cloud sizes of about 0.4–0.8 pc are unaffected by the details of the polytropic approximations. Recently, McLaughlin & Pudritz (1996, 1997) have suggested that the so-called logotropic approximation: $P/P_c = 1 + A\ \ln(\rho/\rho_c)$ for the equation of state provides a better description of the internal structure and average properties of molecular clouds as well as dense clumps of both high and low mass. We have examined the density structure of a dense cloud using the logotropic equations of state. We found with the logotropic approximation an even higher density gradient at the edge of the cloud compared to the polytropic case.

Table 4. Average column densities (in cm^{-2}) of selected species for various beam-radii (in pc) and evolution times (2×10^5, 5×10^5 and 1×10^6 years) in the standard model with CO sticking coefficient S=0.1; $\bar{A}_\mathrm{v}$ is the beam-averaged total A_v. Note: $x(y)$ refers to $x \times 10^y$.

beam-radius [pc]	0.00	0.02	0.05	0.10	0.15	0.20	0.25	0.30	TMC-1
$\bar{A}_\mathrm{v}$ [mags]	8.0	7.9	7.5	6.5	5.4	4.6	3.9	3.3	
C	4.6 (18)	4.6 (18)	4.6 (18)	4.4 (18)	4.0 (18)	3.3 (18)	2.7 (18)	2.1 (18)	
	3.2 (18)	3.3 (18)	3.4 (18)	3.7 (18)	3.7 (18)	3.1 (18)	2.5 (18)	2.0 (18)	$1-10\,(17)$ [1]
	2.8 (18)	2.8 (18)	2.9 (18)	3.3 (18)	3.4 (18)	3.0 (18)	2.5 (18)	1.9 (18)	
CO	3.0 (18)	2.9 (18)	2.5 (18)	1.6 (18)	8.7 (17)	5.0 (17)	3.4 (17)	2.4 (17)	
	3.0 (18)	3.0 (18)	2.6 (18)	1.7 (18)	9.0 (17)	5.2 (17)	3.5 (17)	2.4 (17)	$8-12\,(17)$ [2]
	1.9 (18)	1.9 (18)	1.8 (18)	1.3 (18)	7.2 (17)	4.2 (17)	2.8 (17)	2.0 (17)	
H_2CO	5.5 (14)	4.4 (14)	2.3 (14)	9.0 (13)	4.0 (13)	2.2 (13)	1.5 (13)	1.0 (13)	
	3.9 (14)	3.2 (14)	1.8 (14)	7.5 (13)	3.4 (13)	1.9 (13)	1.2 (13)	8.5 (12)	5 (14) [8]
	5.5 (13)	5.2 (13)	4.7 (13)	3.0 (13)	1.5 (13)	8.2 (12)	5.4 (12)	3.7 (12)	
HCO^+	5.4 (12)	5.1 (12)	3.8 (12)	1.8 (12)	9.1 (11)	5.3 (11)	3.7 (11)	2.6 (11)	
	8.2 (12)	7.9 (12)	6.0 (12)	2.7 (12)	1.3 (12)	7.3 (11)	5.0 (11)	3.4 (11)	$2-4\,(13)$ [2]
	7.7 (12)	7.4 (12)	5.8 (12)	2.6 (12)	1.2 (12)	7.0 (11)	4.7 (11)	3.3 (11)	
CH	1.0 (15)	1.0 (15)	1.0 (15)	1.1 (15)	1.1 (15)	1.1 (15)	1.1 (15)	1.0 (15)	
	8.7 (14)	8.7 (14)	8.8 (14)	9.3 (14)	9.8 (14)	1.0 (15)	9.7 (14)	8.9 (14)	2 (14) [3]
	8.0 (14)	8.0 (14)	8.2 (14)	8.7 (14)	9.4 (14)	9.6 (14)	9.3 (14)	8.4 (14)	
C_2H	1.4 (14)	1.3 (14)	1.3 (14)	1.3 (14)	1.3 (14)	1.2 (14)	1.2 (14)	1.0 (14)	
	1.0 (14)	1.0 (14)	1.0 (14)	1.1 (14)	1.1 (14)	1.1 (14)	1.0 (14)	8.8 (13)	$3-10\,(13)$ [2]
	8.7 (13)	8.8 (13)	9.0 (13)	9.7 (13)	1.0 (14)	1.0 (14)	9.6 (13)	8.4 (13)	
C_3H	1.3 (15)	1.2 (15)	7.7 (14)	3.2 (14)	1.5 (14)	8.2 (13)	5.4 (13)	3.7 (13)	
	8.0 (14)	6.3 (14)	3.7 (14)	1.7 (14)	7.9 (13)	4.5 (13)	3.0 (13)	2.0 (13)	2 (14) [8]
	3.9 (13)	3.8 (13)	4.0 (13)	4.1 (13)	2.6 (13)	1.5 (13)	1.0 (13)	7.2 (12)	
C_4H	1.4 (15)	1.0 (15)	5.0 (14)	1.9 (14)	9.0 (13)	5.3 (13)	3.6 (13)	2.4 (13)	
	1.8 (14)	1.2 (14)	6.9 (13)	3.8 (13)	2.5 (13)	1.7 (13)	1.2 (13)	8.1 (12)	$1-4\,(15)$ [4]
	1.2 (13)	1.2 (13)	1.2 (13)	1.4 (13)	1.4 (13)	1.1 (13)	7.7 (12)	5.4 (12)	
C_3H_2	1.9 (13)	1.8 (13)	1.4 (13)	1.0 (13)	7.6 (12)	5.7 (12)	4.2 (12)	3.0 (12)	
	1.3 (13)	1.1 (13)	9.1 (12)	7.5 (12)	6.3 (12)	4.9 (12)	3.6 (12)	2.6 (12)	1 (14) [3]
	4.7 (12)	4.7 (12)	4.9 (12)	5.5 (12)	5.3 (12)	4.3 (12)	3.2 (12)	2.3 (12)	
CH_3OH	2.0 (13)	1.2 (13)	3.7 (12)	1.2 (12)	4.9 (11)	2.7 (11)	1.8 (11)	1.2 (11)	
	2.2 (13)	1.3 (13)	4.4 (12)	1.4 (12)	5.7 (11)	3.2 (11)	2.1 (11)	1.4 (11)	$2-4\,(13)$ [2]
	2.1 (12)	1.7 (12)	8.3 (11)	3.1 (11)	1.3 (11)	7.3 (10)	4.8 (10)	3.3 (10)	
CN	1.2 (14)	1.2 (14)	1.1 (14)	9.7 (13)	9.2 (13)	7.8 (13)	7.4 (13)	6.5 (13)	
	1.4 (14)	1.3 (14)	1.1 (14)	9.7 (13)	9.2 (13)	7.2 (13)	6.8 (13)	5.8 (13)	3 (14) [3]
	1.1 (14)	1.1 (14)	1.2 (14)	1.1 (14)	1.0 (14)	7.4 (13)	6.8 (13)	5.8 (13)	
HCN	3.0 (14)	2.0 (14)	8.5 (13)	3.6 (13)	1.7 (13)	9.5 (12)	6.4 (12)	4.4 (12)	
	2.3 (14)	1.3 (14)	5.3 (13)	2.4 (13)	1.2 (13)	6.6 (12)	4.4 (12)	3.0 (12)	2 (14) [3]
	5.0 (13)	3.8 (13)	2.1 (13)	1.2 (13)	6.1 (12)	3.5 (12)	2.4 (12)	1.6 (12)	
HC_3N	8.9 (13)	4.7 (13)	1.2 (13)	3.8 (12)	1.6 (12)	9.1 (11)	6.1 (11)	4.2 (11)	
	4.5 (13)	1.9 (13)	4.6 (12)	1.4 (12)	6.4 (11)	3.5 (11)	2.4 (11)	1.6 (11)	6 (13) [3]
	2.2 (11)	1.2 (11)	9.0 (10)	6.9 (10)	4.6 (10)	2.9 (10)	1.9 (10)	1.3 (10)	1.7 (14) [5]
CH_3CN	2.0 (13)	1.0 (13)	2.8 (12)	8.8 (11)	3.7 (11)	2.1 (11)	1.4 (11)	9.4 (10)	
	1.4 (13)	6.6 (12)	1.9 (12)	6.1 (11)	2.6 (11)	1.4 (11)	9.5 (10)	6.5 (10)	5 (12) [6]
	2.3 (11)	2.0 (11)	1.4 (11)	7.0 (10)	3.0 (10)	1.7 (10)	1.1 (10)	7.6 (09)	
NH_3	1.6 (13)	1.4 (13)	8.1 (12)	3.3 (12)	1.5 (12)	8.2 (11)	5.4 (11)	3.7 (11)	
	5.2 (13)	4.3 (13)	2.3 (13)	8.9 (12)	3.9 (12)	2.1 (12)	1.4 (12)	9.7 (11)	2 (14) [5]
	1.8 (14)	1.4 (14)	6.8 (13)	2.4 (13)	1.0 (13)	5.7 (12)	3.8 (12)	2.6 (12)	
N_2H^+	2.5 (11)	2.4 (11)	1.7 (11)	8.2 (10)	3.8 (10)	2.1 (10)	1.4 (10)	9.6 (09)	
	9.6 (11)	9.2 (11)	6.7 (11)	2.9 (11)	1.3 (11)	7.2 (10)	4.8 (10)	3.2 (10)	5 (12) [3]
	2.2 (12)	2.1 (12)	1.6 (12)	6.5 (11)	2.8 (11)	1.6 (11)	1.0 (11)	7.2 (10)	1 (13) [7]
CS	8.3 (15)	8.6 (15)	9.6 (15)	7.7 (15)	4.2 (15)	2.6 (15)	1.8 (15)	1.2 (15)	
	7.6 (15)	7.9 (15)	8.8 (15)	7.0 (15)	3.9 (15)	2.4 (15)	1.6 (15)	1.1 (15)	1 (14) [3]
	6.5 (15)	6.8 (15)	7.5 (15)	5.9 (15)	3.4 (15)	2.1 (15)	1.5 (15)	1.0 (15)	
C_2S	7.8 (13)	8.0 (13)	1.3 (14)	8.9 (13)	8.6 (13)	4.8 (13)	2.8 (13)	1.9 (13)	
	1.0 (14)	1.1 (14)	1.7 (14)	1.2 (14)	1.0 (14)	5.5 (13)	3.2 (13)	2.1 (13)	1 (14) [4]
	8.5 (13)	8.8 (13)	9.4 (13)	9.8 (13)	9.9 (13)	5.3 (13)	3.0 (13)	2.0 (13)	
C_3S	1.6 (13)	1.6 (13)	1.7 (13)	1.5 (13)	7.8 (12)	4.4 (12)	3.0 (12)	2.0 (12)	
	1.2 (13)	1.3 (13)	1.4 (13)	1.2 (13)	6.7 (12)	3.8 (12)	2.6 (12)	1.8 (12)	$2 \pm 0.4\,(13)$ [4]
	7.1 (12)	7.1 (12)	7.8 (12)	9.0 (12)	5.2 (12)	3.0 (12)	2.0 (12)	1.4 (12)	
HCS^+	6.3 (11)	6.5 (11)	7.1 (11)	5.8 (11)	4.1 (11)	3.0 (11)	2.3 (11)	1.7 (11)	
	7.3 (11)	7.6 (11)	8.4 (11)	6.3 (11)	4.2 (11)	3.0 (11)	2.2 (11)	1.7 (11)	$1 \pm 0.3\,(13)$ [4]
	6.8 (11)	7.0 (11)	7.7 (11)	5.8 (11)	4.0 (11)	2.8 (11)	2.2 (11)	1.6 (11)	
SO	6.0 (11)	6.0 (11)	6.4 (11)	7.5 (11)	6.9 (11)	5.0 (11)	3.6 (11)	2.6 (11)	
	9.2 (11)	9.4 (11)	1.0 (12)	1.0 (12)	8.2 (11)	5.7 (11)	4.1 (11)	2.9 (11)	5 (13) [3]
	2.0 (13)	2.1 (13)	1.5 (13)	5.8 (12)	2.8 (12)	1.7 (12)	1.2 (12)	8.0 (11)	

[1] Schilke et al. (1995), [2] Pratap et al. (1997), [3] Ohishi et al. (1992), [4] Hirahara et al. (1992)
[5] Suzuki et al. (1992), [6] Minh et al. (1993), [7] Hirahara et al. (1995), [8] Ohishi & Kaifu (1998)

This discrepancy will not produce a significant difference in the overall frame of the chemistry nor in the predicted chemical abundances and the column densities for low mass dense cloud cores.

The effect of internally generated UV photons by cosmic rays on the chemical evolution of the cloud at early times is significant. The dominant effect of cosmic-ray-induced photons on the chemistry is via increasing the fractional ionization of the gas by, most importantly, increasing the abundance of C^+. This effect is mainly confined to the first half a million years and to the inner parts of the cloud close to the centre (i.e. covering a radius equivalent to an A_v of 3 mag). The effect of the increase in C^+ abundance is particularly important for abundances of carbon-chain nitrogen (e.g. HCN, HC_3N, CH_3CN),

Table 5. Local abundances (relative to hydrogen) of selected species for various distances r (in pc) from the cloud centre and evolution times (2×10^5, 5×10^5 and 1×10^6 years) in the standard model with CO sticking coefficient $S = 0.1$; the total cloud radius is $R = 0.64$ pc and $A_v(r)$ is the local A_v at a radial depth $R - r$ from the cloud surface. The quoted observed abundances are derived from observed column densities by dividing with a total hydrogen number density $N_H = 1 \times 10^{22} cm^{-2}$. Note: $x(y)$ refers to $x \times 10^y$.

r [pc]	0.00	0.02	0.03	0.05	0.07	0.10	0.13	0.20	TMC-1
A_v(r) [mags]	8.0	6.9	6.2	5.2	4.7	3.6	2.8	1.8	
	9.8 (-05)	1.1 (-04)	1.2 (-04)	1.3 (-04)	1.6 (-04)	2.5 (-04)	3.2 (-04)	3.2 (-04)	
C	1.3 (-05)	1.5 (-05)	1.9 (-05)	3.0 (-05)	5.8 (-05)	2.0 (-04)	3.2 (-04)	3.2 (-04)	$1 - 10$ (-05) [1]
	7.1 (-08)	1.7 (-07)	4.2 (-07)	1.9 (-06)	1.6 (-05)	1.7 (-04)	3.0 (-04)	3.2 (-04)	
	2.1 (-04)	2.1 (-04)	2.1 (-04)	2.0 (-04)	1.8 (-04)	1.1 (-04)	4.1 (-05)	8.4 (-06)	
CO	1.9 (-04)	2.0 (-04)	2.0 (-04)	2.1 (-04)	2.0 (-04)	1.2 (-04)	3.8 (-05)	7.6 (-06)	$8 - 12$ (-05) [2]
	1.0 (-04)	1.1 (-04)	1.1 (-04)	1.3 (-04)	1.4 (-04)	1.0 (-04)	3.7 (-05)	7.5 (-06)	
	1.2 (-07)	6.1 (-08)	3.6 (-08)	1.9 (-08)	9.6 (-09)	1.7 (-09)	4.0 (-10)	3.3 (-11)	
H_2CO	9.0 (-08)	4.0 (-08)	2.6 (-08)	1.6 (-08)	9.0 (-09)	1.7 (-09)	4.0 (-10)	3.3 (-11)	5 (-08) [8]
	5.1 (-09)	3.5 (-09)	3.3 (-09)	3.7 (-09)	4.7 (-09)	1.7 (-09)	4.1 (-10)	3.3 (-11)	
	5.7 (-10)	5.1 (-10)	4.5 (-10)	3.6 (-10)	2.4 (-10)	6.0 (-11)	2.6 (-11)	9.0 (-12)	
HCO^+	7.9 (-10)	7.7 (-10)	7.5 (-10)	6.5 (-10)	3.7 (-10)	6.4 (-11)	2.6 (-11)	8.4 (-12)	$2 - 4$ (-09) [2]
	6.8 (-10)	7.0 (-10)	7.2 (-10)	6.5 (-10)	3.2 (-10)	6.3 (-11)	2.6 (-11)	8.3 (-12)	
	6.5 (-09)	7.2 (-09)	8.0 (-09)	9.5 (-09)	1.2 (-08)	1.8 (-08)	3.3 (-08)	1.1 (-07)	
CH	1.4 (-09)	1.5 (-09)	2.0 (-09)	3.2 (-09)	5.9 (-09)	1.6 (-08)	3.2 (-08)	9.6 (-08)	2 (-08) [3]
	2.5 (-11)	4.0 (-11)	8.5 (-11)	3.2 (-10)	2.2 (-09)	1.5 (-08)	3.1 (-08)	9.4 (-08)	
	2.2 (-09)	2.1 (-09)	2.2 (-09)	2.6 (-09)	3.1 (-09)	3.5 (-09)	5.0 (-09)	1.3 (-08)	
C_2H	8.2 (-10)	4.6 (-10)	5.0 (-10)	8.0 (-10)	1.3 (-09)	2.9 (-09)	4.8 (-09)	1.2 (-08)	$3 - 10$ (-09) [2]
	2.8 (-11)	3.1 (-11)	6.4 (-11)	1.9 (-10)	4.6 (-10)	2.3 (-09)	4.7 (-09)	1.2 (-08)	
	1.8 (-07)	1.4 (-07)	1.1 (-07)	7.4 (-08)	4.2 (-08)	6.3 (-09)	2.0 (-09)	4.4 (-10)	
C_3H	1.9 (-07)	7.7 (-08)	5.0 (-08)	3.3 (-08)	1.9 (-08)	5.2 (-09)	2.0 (-09)	4.0 (-10)	2 (-08) [8]
	3.0 (-09)	5.5 (-10)	5.6 (-10)	1.1 (-09)	3.5 (-09)	4.3 (-09)	1.9 (-09)	4.0 (-10)	
	4.0 (-07)	1.5 (-07)	8.2 (-08)	4.0 (-08)	1.7 (-08)	2.3 (-09)	1.6 (-09)	1.2 (-09)	
C_4H	6.1 (-08)	1.5 (-08)	7.7 (-09)	4.6 (-09)	3.2 (-09)	1.6 (-09)	1.5 (-09)	1.1 (-09)	$1 - 4$ (-07) [4]
	5.9 (-10)	5.0 (-11)	2.1 (-11)	3.6 (-11)	2.0 (-10)	1.0 (-09)	1.4 (-09)	1.1 (-09)	
	2.0 (-09)	1.4 (-09)	1.1 (-09)	9.0 (-10)	7.5 (-10)	4.7 (-10)	5.2 (-10)	5.4 (-10)	
C_3H_2	2.3 (-09)	7.6 (-10)	5.1 (-10)	4.1 (-10)	3.9 (-10)	4.0 (-10)	5.0 (-10)	4.9 (-10)	1 (-08) [3]
	1.0 (-10)	1.7 (-11)	1.8 (-11)	3.6 (-11)	1.3 (-10)	3.3 (-10)	4.9 (-10)	4.8 (-10)	
	7.7 (-09)	2.0 (-09)	6.7 (-10)	1.7 (-10)	4.3 (-11)	2.2 (-12)	1.4 (-13)	9.0 (-16)	
CH_3OH	9.0 (-09)	2.1 (-09)	8.0 (-10)	2.3 (-10)	5.5 (-11)	2.4 (-12)	1.4 (-13)	8.8 (-16)	$2 - 4$ (-09) [2]
	5.3 (-10)	2.4 (-10)	1.3 (-10)	6.8 (-11)	3.7 (-11)	2.7 (-12)	1.5 (-13)	8.9 (-16)	
	5.3 (-09)	5.1 (-09)	4.7 (-09)	4.2 (-09)	3.8 (-09)	3.1 (-09)	2.9 (-09)	7.1 (-09)	
CN	1.1 (-08)	6.8 (-09)	5.6 (-09)	4.9 (-09)	4.5 (-09)	3.5 (-09)	3.0 (-09)	6.5 (-09)	3 (-08) [3]
	6.6 (-10)	1.6 (-09)	3.1 (-09)	5.8 (-09)	8.2 (-09)	4.5 (-09)	3.1 (-09)	6.4 (-09)	
	9.8 (-08)	3.0 (-08)	1.2 (-08)	5.4 (-09)	3.1 (-09)	1.4 (-09)	3.4 (-10)	4.6 (-11)	
HCN	1.0 (-07)	1.8 (-08)	6.6 (-09)	3.2 (-09)	2.2 (-09)	1.1 (-09)	3.0 (-10)	4.1 (-11)	2 (-08) [3]
	1.3 (-08)	4.9 (-09)	2.9 (-09)	1.4 (-09)	8.1 (-10)	7.8 (-10)	2.9 (-10)	4.0 (-11)	
	4.1 (-08)	7.7 (-09)	2.0 (-09)	4.2 (-10)	1.1 (-10)	1.5 (-11)	5.4 (-12)	9.7 (-13)	
HC_3N	2.9 (-08)	2.8 (-09)	6.4 (-10)	1.3 (-10)	4.1 (-11)	1.0 (-11)	4.8 (-12)	8.8 (-13)	6 (-09) [3]
	1.6 (-10)	7.6 (-12)	5.8 (-12)	5.2 (-12)	5.0 (-12)	5.4 (-12)	4.4 (-12)	8.7 (-13)	1.7 (-08) [5]
	9.0 (-09)	1.7 (-09)	4.4 (-10)	1.1 (-10)	3.3 (-11)	2.8 (-12)	1.4 (-13)	1.9 (-15)	
CH_3CN	8.2 (-09)	9.7 (-10)	2.7 (-10)	9.2 (-11)	3.3 (-11)	2.5 (-12)	1.2 (-13)	1.6 (-15)	5 (-10) [6]
	4.4 (-11)	2.0 (-11)	1.7 (-11)	1.4 (-11)	1.0 (-12)	2.0 (-12)	1.2 (-13)	1.6 (-15)	
	3.1 (-09)	1.8 (-09)	1.2 (-09)	7.3 (-10)	3.9 (-10)	7.4 (-11)	1.7 (-11)	4.0 (-13)	
NH_3	1.0 (-08)	5.9 (-09)	3.8 (-09)	2.1 (-09)	9.2 (-10)	1.4 (-10)	2.8 (-11)	3.8 (-13)	2 (-08) [5]
	4.3 (-08)	2.1 (-08)	1.2 (-08)	5.5 (-09)	2.0 (-09)	2.5 (-10)	3.6 (-11)	3.8 (-13)	
	2.6 (-11)	2.4 (-11)	2.2 (-11)	1.7 (-11)	1.1 (-11)	2.7 (-12)	7.9 (-13)	8.6 (-14)	
N_2H^+	1.0 (-10)	9.4 (-11)	8.7 (-11)	7.1 (-11)	4.0 (-11)	6.7 (-12)	1.5 (-12)	8.1 (-14)	5 (-10) [3]
	2.2 (-10)	2.2 (-10)	2.1 (-10)	1.7 (-10)	8.6 (-11)	1.3 (-11)	1.9 (-12)	8.0 (-14)	1 (-09) [7]
	3.1 (-08)	1.5 (-07)	3.4 (-07)	6.5 (-07)	9.2 (-07)	5.6 (-07)	2.1 (-07)	8.1 (-08)	
CS	3.0 (-08)	1.5 (-07)	3.4 (-07)	6.2 (-07)	8.4 (-07)	5.1 (-07)	2.1 (-07)	7.4 (-08)	1 (-08) [3]
	8.0 (-09)	1.4 (-07)	3.1 (-07)	5.3 (-07)	6.4 (-07)	4.6 (-07)	2.0 (-07)	7.4 (-08)	
	3.9 (-10)	1.0 (-09)	1.8 (-09)	3.6 (-09)	8.2 (-09)	8.7 (-09)	2.4 (-09)	4.7 (-10)	
C_2S	5.3 (-10)	1.7 (-09)	3.2 (-09)	6.8 (-09)	1.2 (-08)	9.0 (-09)	2.4 (-09)	4.3 (-10)	1 (-08) [4]
	4.1 (-10)	6.9 (-10)	1.0 (-09)	3.0 (-09)	1.1 (-08)	9.5 (-09)	2.4 (-09)	4.2 (-10)	
	1.8 (-10)	3.9 (-10)	5.6 (-10)	9.2 (-10)	1.7 (-09)	1.3 (-09)	3.5 (-10)	3.6 (-11)	
C_3S	1.5 (-10)	2.6 (-10)	3.8 (-10)	6.9 (-10)	1.4 (-09)	1.2 (-09)	3.4 (-10)	3.3 (-11)	2 ± 0.4 (-09) [4]
	5.6 (-11)	4.4 (-11)	3.6 (-11)	9.2 (-11)	6.0 (-11)	1.1 (-09)	3.4 (-10)	3.3 (-11)	
	1.8 (-12)	1.0 (-11)	2.6 (-11)	4.5 (-11)	5.1 (-11)	3.7 (-11)	2.9 (-11)	2.1 (-11)	
HCS^+	2.3 (-12)	1.4 (-11)	3.5 (-11)	6.7 (-11)	6.4 (-11)	3.7 (-11)	2.9 (-11)	1.9 (-11)	1 ± 0.3 (-09) [4]
	2.5 (-12)	1.3 (-11)	3.4 (-11)	6.2 (-11)	5.1 (-11)	3.6 (-11)	2.9 (-11)	1.9 (-11)	
	8.1 (-14)	3.9 (-13)	9.6 (-13)	3.1 (-12)	1.2 (-11)	6.5 (-11)	7.7 (-11)	4.0 (-11)	
SO	1.6 (-12)	6.5 (-12)	1.4 (-11)	2.9 (-11)	5.9 (-11)	8.4 (-11)	7.9 (-11)	3.9 (-11)	5 (-09) [3]
	8.0 (-10)	2.2 (-09)	2.7 (-09)	1.6 (-09)	4.2 (-10)	1.1 (-10)	8.2 (-11)	3.9 (-11)	

[1] Schilke et al. (1995), [2] Pratap et al. (1997), [3] Ohishi et al. (1992), [4] Hirahara et al. (1992)
[5] Suzuki et al. (1992), [6] Minh et al. (1993), [7] Hirahara et al. (1995), [8] Ohishi & Kaifu (1998)

and carbon-chain sulphur containing species (e.g. C_2S), whose predicted abundances are found to be in much closer agreement with observations in the presence of CRI photons. The high sensitivity of the abundances of HCN, HC_3N, CH_3CN, CH_3CN and C_2S to the influence of CRI photons, suggests that these molecules could be quite useful as probes of radiative processes and the strength of the local cosmic ray flux. The chemical abundances at later times are less directly affected by cosmic-ray-induced photons. However, cosmic rays significantly affect the abundances at later times of the cloud evolution by direct heating of dust grains and the consequent desorption of CO from grain mantles.

It appears that, while the abundance ratio of C/CO is greater than 1, the chemistry of carbon-containing species is develop-

Table 6. Average column densities (in cm^{-2}) of selected species for various beam-radii (in pc) and evolution times (2×10^5, 5×10^5 and 1×10^6 years) in the standard model with a two sided external UV radiation field in the direction of the observer; $\bar{A}_\mathrm{v}$ is the beam-averaged total A_v. Note: $x(y)$ refers to $x \times 10^y$.

beam-radius [pc]	0.00	0.02	0.05	0.10	0.15	0.20	0.25	0.30	TMC-1
$\bar{A}_\mathrm{v}$ [mags]	8.0	7.9	7.5	6.5	5.4	4.6	3.9	3.3	
C	4.5 (18)	4.5 (18)	4.4 (18)	4.2 (18)	3.7 (18)	3.2 (18)	2.7 (18)	2.2 (18)	
	2.9 (18)	2.9 (18)	3.0 (18)	3.0 (18)	3.0 (18)	2.7 (18)	2.4 (18)	2.0 (18)	$1-10\,(17)$ [1]
	2.4 (18)	2.4 (18)	2.4 (18)	2.4 (18)	2.5 (18)	2.4 (18)	2.2 (18)	1.9 (18)	
CO	2.1 (18)	2.1 (18)	1.9 (18)	1.4 (18)	9.0 (17)	5.7 (17)	4.0 (17)	2.8 (17)	
	1.4 (18)	1.3 (18)	1.3 (18)	1.1 (18)	7.6 (17)	4.9 (17)	3.4 (17)	2.4 (17)	$8-12\,(17)$ [2]
	5.3 (17)	5.3 (17)	5.3 (17)	5.3 (17)	4.5 (17)	3.1 (17)	2.2 (17)	1.5 (17)	
H_2CO	6.7 (14)	6.2 (14)	4.1 (14)	1.8 (14)	8.4 (13)	4.7 (13)	3.1 (13)	2.1 (13)	
	4.2 (14)	4.0 (14)	3.2 (14)	1.7 (14)	8.0 (13)	4.5 (13)	3.0 (13)	2.0 (13)	5 (14) [8]
	2.5 (13)	2.4 (13)	2.2 (13)	1.8 (13)	1.3 (13)	7.7 (12)	5.2 (12)	3.6 (12)	
HCO^+	4.9 (12)	4.8 (12)	4.1 (12)	2.6 (12)	1.4 (12)	8.6 (11)	6.0 (11)	4.2 (11)	
	5.7 (12)	5.6 (12)	5.3 (12)	3.7 (12)	2.0 (12)	1.2 (12)	7.9 (11)	5.5 (11)	$2-4\,(13)$ [2]
	2.6 (12)	2.7 (12)	2.7 (12)	2.4 (12)	1.4 (12)	8.3 (11)	5.8 (11)	4.1 (11)	
CH	1.0 (15)	1.0 (15)	1.0 (15)	1.0 (15)	1.0 (15)	9.8 (14)	9.5 (14)	9.0 (14)	
	8.5 (14)	8.5 (14)	8.5 (14)	8.6 (14)	8.7 (14)	8.5 (14)	8.2 (14)	7.7 (14)	2 (14) [3]
	7.7 (14)	7.7 (14)	7.7 (14)	7.8 (14)	8.0 (14)	7.9 (14)	7.7 (14)	7.2 (14)	
C_2H	1.3 (14)	1.3 (14)	1.3 (14)	1.3 (14)	1.2 (14)	1.1 (14)	1.0 (14)	9.3 (13)	
	9.5 (13)	9.5 (13)	9.5 (13)	9.6 (13)	9.5 (13)	9.1 (13)	8.6 (13)	7.8 (13)	$3-10\,(13)$ [2]
	8.1 (13)	8.1 (13)	8.1 (13)	8.2 (13)	8.4 (13)	8.2 (13)	7.9 (13)	7.2 (13)	
C_3H	1.4 (15)	1.3 (15)	1.0 (15)	5.8 (14)	2.8 (14)	1.5 (14)	1.0 (14)	7.1 (13)	
	5.6 (14)	5.3 (14)	4.0 (14)	2.5 (14)	1.2 (14)	7.2 (13)	4.8 (13)	3.3 (13)	2 (14) [8]
	1.3 (13)	1.3 (13)	1.2 (13)	1.3 (13)	1.3 (13)	9.6 (12)	7.0 (12)	4.9 (12)	
C_4H	1.4 (15)	1.3 (15)	9.3 (14)	4.5 (14)	2.1 (14)	1.2 (14)	8.0 (13)	5.5 (13)	
	7.3 (13)	6.8 (13)	5.4 (13)	4.1 (13)	2.6 (13)	1.7 (13)	1.3 (13)	9.0 (12)	$1-4\,(15)$ [4]
	8.5 (12)	8.4 (12)	7.9 (12)	7.7 (12)	7.7 (12)	7.0 (12)	5.8 (12)	4.4 (12)	
C_3H_2	1.9 (13)	1.9 (13)	1.7 (13)	1.3 (13)	8.7 (12)	6.4 (12)	4.9 (12)	3.7 (12)	
	9.8 (12)	9.4 (12)	8.3 (12)	7.2 (12)	5.8 (12)	4.6 (12)	3.7 (12)	2.8 (12)	1 (14) [3]
	3.4 (12)	3.4 (12)	3.4 (12)	3.5 (12)	3.6 (12)	3.3 (12)	2.8 (12)	2.2 (12)	
CH_3OH	2.8 (13)	2.4 (13)	1.2 (13)	4.0 (12)	1.7 (12)	9.4 (11)	6.3 (11)	4.3 (11)	
	2.6 (13)	2.4 (13)	1.5 (13)	6.0 (12)	2.6 (12)	1.4 (12)	9.5 (11)	6.5 (11)	$2-4\,(13)$ [2]
	7.2 (11)	6.7 (11)	4.6 (11)	2.6 (11)	1.3 (11)	7.1 (10)	4.7 (10)	3.2 (10)	
CN	1.3 (14)	1.2 (14)	1.2 (14)	1.0 (14)	8.4 (13)	7.4 (13)	6.7 (13)	6.1 (13)	
	1.6 (14)	1.6 (14)	1.4 (14)	1.1 (14)	8.7 (13)	7.3 (13)	6.4 (13)	5.7 (13)	3 (14) [3]
	8.6 (13)	8.6 (13)	8.7 (13)	8.7 (13)	7.9 (13)	6.8 (13)	6.0 (13)	5.4 (13)	
HCN	3.5 (14)	3.2 (14)	1.8 (14)	7.5 (13)	3.6 (13)	2.0 (13)	1.4 (13)	9.4 (12)	
	3.4 (14)	3.0 (14)	1.7 (14)	7.3 (13)	3.4 (13)	2.0 (13)	1.3 (13)	9.0 (12)	2 (14) [3]
	8.0 (13)	7.5 (13)	5.4 (13)	2.9 (13)	1.5 (13)	8.9 (12)	6.0 (12)	4.2 (12)	
HC_3N	1.0 (14)	8.8 (13)	4.2 (13)	1.4 (13)	6.2 (12)	3.4 (12)	2.3 (12)	1.6 (12)	
	3.8 (13)	3.2 (13)	1.5 (13)	5.4 (12)	2.3 (12)	1.3 (12)	8.6 (11)	5.9 (11)	6 (13) [3]
	3.4 (10)	3.2 (10)	2.7 (10)	2.7 (10)	2.8 (10)	2.2 (10)	1.6 (10)	1.1 (10)	1.7 (14) [5]
CH_3CN	2.6 (13)	2.2 (13)	1.0 (13)	3.3 (12)	1.4 (12)	7.8 (11)	5.2 (11)	3.5 (11)	
	1.9 (13)	1.7 (12)	9.8 (12)	3.6 (11)	1.6 (12)	8.6 (11)	5.7 (11)	3.9 (11)	5 (12) [6]
	1.3 (11)	1.2 (11)	1.1 (11)	9.0 (10)	5.3 (10)	2.9 (10)	2.0 (10)	1.3 (10)	
NH_3	2.9 (13)	2.8 (13)	2.1 (13)	1.0 (13)	4.6 (12)	2.6 (12)	1.7 (12)	1.2 (12)	
	1.9 (14)	1.8 (14)	1.3 (14)	5.8 (13)	2.6 (13)	1.4 (13)	9.4 (12)	6.4 (12)	2 (14) [5]
	6.2 (14)	5.9 (14)	4.2 (14)	1.9 (14)	8.4 (13)	4.6 (13)	3.1 (13)	2.1 (13)	
N_2H^+	3.3 (11)	3.1 (11)	2.5 (11)	1.4 (11)	7.2 (10)	4.2 (10)	2.8 (10)	1.9 (10)	
	2.1 (12)	2.0 (12)	1.6 (12)	9.1 (11)	4.3 (11)	2.4 (11)	1.6 (11)	1.1 (11)	5 (12) [3]
	4.7 (12)	4.6 (12)	4.1 (12)	2.7 (12)	1.3 (12)	7.1 (11)	4.7 (11)	3.2 (11)	1 (13) [7]
CS	8.2 (15)	8.6 (15)	1.0 (16)	1.0 (16)	7.2 (15)	4.5 (15)	3.1 (15)	2.2 (15)	
	7.2 (15)	7.6 (15)	9.0 (15)	9.2 (15)	6.5 (15)	4.1 (15)	2.8 (15)	2.0 (15)	1 (14) [3]
	5.3 (15)	5.6 (15)	6.7 (15)	6.8 (15)	4.9 (15)	3.2 (15)	2.2 (15)	1.6 (15)	
C_2S	8.4 (13)	8.6 (13)	9.2 (13)	8.6 (13)	6.3 (13)	4.0 (13)	2.7 (13)	1.9 (13)	
	1.2 (14)	1.2 (14)	1.4 (14)	1.3 (14)	8.2 (13)	5.0 (13)	3.4 (13)	2.4 (13)	1 (14) [4]
	6.4 (13)	6.7 (13)	7.4 (13)	7.6 (13)	6.0 (13)	3.8 (13)	2.6 (13)	1.8 (13)	
C_3S	1.7 (13)	1.8 (13)	2.0 (13)	1.8 (13)	1.2 (13)	7.1 (12)	4.8 (12)	3.3 (12)	
	1.2 (13)	1.2 (13)	1.4 (13)	1.4 (13)	9.5 (12)	5.8 (12)	3.9 (12)	2.7 (12)	$2 \pm 0.4\,(13)$ [4]
	4.4 (12)	4.6 (12)	5.0 (12)	5.0 (12)	4.5 (12)	3.0 (12)	2.1 (12)	1.4 (12)	
HCS^+	6.4 (11)	6.6 (11)	7.4 (11)	7.1 (11)	5.4 (11)	4.0 (11)	3.2 (11)	2.4 (11)	
	7.6 (11)	7.9 (11)	9.3 (11)	9.1 (11)	6.4 (11)	4.5 (11)	3.4 (11)	2.6 (11)	$1 \pm 0.3\,(13)$ [4]
	7.1 (11)	7.4 (11)	8.9 (11)	9.1 (11)	6.2 (11)	4.5 (11)	3.4 (11)	2.5 (11)	
SO	6.2 (11)	6.2 (11)	6.3 (11)	6.6 (11)	6.6 (11)	5.6 (11)	4.4 (11)	3.3 (11)	
	1.5 (12)	1.6 (12)	1.6 (12)	1.3 (12)	1.0 (12)	7.8 (11)	5.9 (11)	4.3 (11)	5 (13) [3]
	2.5 (14)	2.8 (14)	3.4 (14)	1.9 (14)	8.3 (13)	4.6 (13)	3.0 (13)	2.1 (13)	

[1] Schilke et al. (1995), [2] Pratap et al. (1997), [3] Ohishi et al. (1992), [4] Hirahara et al. (1992)
[5] Suzuki et al. (1992), [6] Minh et al. (1993), [7] Hirahara et al. (1995), [8] Ohishi & Kaifu (1998)

ing; hydrocarbons, carbon-chain nitrogen and carbon-chain sulphur containing molecules are actively produced. The timescale at which C/CO~ 1 coincides approximately with the time when the peak abundances of "early type" species are reached ($\lesssim$ half a million years). When the C/CO abundance ratio becomes less than 1, the chemistry slows down and the chemical equilibrium is reached as early as $t \lesssim 10^6$ years. The timescale for CO accretion onto grains corresponds approximately to the time when C/CO~ 1; therefore, the CO depletion onto grains appears to be the key mechanism for controlling the chemistry at late times of the cloud evolution. The reason for the vital role of CO depletion on the chemistry, particularly at later times, is related to the

loss of CO in the gas phase which in turn changes the ion structure of the chemistry mainly by increasing the amount of H_3^+ available for reactions with non-carbon containing molecules. In the absence of CO accretion, from about half a million years onwards, the main loss of H_3^+ is via reaction with CO in the sequence $CO \xrightarrow{H_3^+} HCO^+ \xrightarrow{e} CO$, which will execute effectively for the remaining time of the chemical evolution, working as an "H_3^+ trap" inhibiting vital ion-molecule reactions for the formation of species like NH_3. With the loss of CO onto grains, the loss of H_3^+ becomes mainly via reaction with atomic oxygen, producing OH^+, H_2O^+ and H_3O^+ (thus enhancing the production of OH and H_2O), and reaction with N_2, producing N_2H^+ and thus NH_3. Therefore, the CO depletion onto grains appears to be the key mechanism for activating the chemistry after the first half a million years; allowing molecules whose evolution is on a timescale of the order 1 million years to reach the appropriate conditions under which they can evolve. The results indicate that considerations of grain accretion processes are crucial in understanding the late stages of the cloud evolution and the conditions in which low mass stars are formed. Desorption processes equally play a critical part in maintaining the chemical balance at the late times of the cloud evolution, thus allowing a gas phase chemical equilibrium to be established in about 5 million years, i.e. a typical "age" for low mass dark clouds.

The sensitivity of the chemistry during late time of the cloud evolution to the CO accretion and desorption rates underlines the importance of these processes. Furthermore, model assumptions should allow for time and depth dependent properties of dust grains and sticking probabilities for different species.

The large observed column density of NH_3 cannot be explained in the context of a pure gas-phase chemistry. The predicted column density of NH_3 in our model is in good agreement with observations when CO grain accretion is included, i.e. this mechanism provides the appropriate C:O:N ratio which appears to be required for the formation of a large abundance of ammonia. In the literature several mechanisms have been proposed for increasing the gas phase abundance of NH_3 in order to reproduce observed values; e.g. removing NH_3-rich ice mantles via continuous and intermittent desorption processes as well as direct grain surface reactions leading to the formation of NH_3. However, Whittet (1993) argues that, although models predict significant quantities of ammonia in the hydrogen-rich component of the mantles, there is little direct evidence for the presence of NH_3 in the ices. Furthermore, as yet there is no data available from ISO observations which indicate the presence of NH_3 or any other (abundant) N-bearing ices (Whittet et al. 1996; Tielens & Whittet 1997; van Dishoeck 1998). From the predicted abundances of NH_3 in the gas phase it also seems unlikely that a significant amount of ammonia can be accreted onto grains to form solid ice mantles, within the accretion timescale of a few$\times 10^5$ years. The most abundant gas phase N-containing species which could be considered for direct accretion on grains are atomic N and N_2 with predicted column densities of about 10^{18} cm^{-2} and 10^{17} cm^{-2}, respectively. Similarly, the direct freeze-out of gas phase H_2O, CO_2 and CH_4 within the required accretion timescale is insufficient to explain the observed ices of these molecules. Hence, the recent ISO-SWS observations of solid H_2O, CO_2 and CH_4 have provided strong evidence for grain surface-chemistry (van Dishoeck 1998). Atomic O, with a predicted column density of about 10^{19} cm^{-2}, appears to be a good candidate for grain accretion and surface reactions; however, the predicted column density of O_2 (of a few$\times 10^{14}$ cm^{-2}at 10^5 years) is too low to allow for a significant accretion of O_2 onto grains. The observation of important molecules like N_2 and O_2 in gas or solid phase will provide key constraints for improving the model assumptions and it will also provide powerful diagnostics for gas-phase and the grain-surface processes (Whittet et al. 1996).

Our results show that adopting a depth dependent sulphur abundance leads to predicted column densities of sulphur-containing species which overall are in closer agreement with observations compared to the case of a fixed sulphur abundance throughout the cloud. In addition, adopting a time dependent sulphur depletion, considering grain surface reactions and appropriate desorption processes involving sulphur species, may help to resolve some of the problems associated with sulphur chemistry in dense molecular cloud models.

Species which are formed in spatially extended regions in the cloud also appear to be extended over the duration of the cloud evolution, e.g. CO, HCO^+, C_2H, C_3H_2, CS and HCS^+. This group of species can be studied in the context of depth and time dependent models to diagnose the conditions in both dense and translucent clouds.

It should be noted that, although the spherical models studied in this work allow a 1-D/2-D spatial distribution of abundances to be considered for comparison with observations, nevertheless most of our results and conclusions were found considering the time dependent variation of abundance profiles along the central line of sight. The study of a time and depth dependent chemistry restricted to the central line of sight is in most cases sufficient for predicting abundances and column densities which can be compared with observations. However, for species which are concentrated in the densest part of the cloud core, e.g. HC_3N and CH_3CN, beam averaged column densities provide a more meaningful comparison. We also showed that the geometry of the external UV radiation field can have a significant influence on the observed beam averaged column densities of these "core species".

Our time and depth dependent models highlight the effects of a few physical and chemical processes which time dependent one-point models alone cannot adequately display. Applications of such models with an improved treatment of the physics, dynamics and a combined gas and grain surface chemistry will hopefully provide a better understanding of the chemical composition and the properties of dense molecular cloud cores and low mass star-forming regions.

Acknowledgements. We are grateful to D.A. Williams for reading the manuscript and helpful comments, in particular for suggesting a depth dependent sulphur abundance. We would like to thank T.W. Hartquist for discussions and comments on the manuscript. We gratefully thank the referee for helpful comments. We thank S. Lynch for discussions

on nonlinearity and bistability and M. Holme for valuable technical support. Lida Nejad acknowledges the support of PPARC for the computing grant GR/J67574.

References

Adams N.G., Smith D., 1987, ApJ 317, L25
Bennett A., 1988, Rate coefficients in Astrochemistry. Kluwer, Dordrecht, p. 339
Benson P.J., 1986, Masers, Molecules, and Mass Outflows in Star Forming Regions. Haystack Observatory, Westford, MA, p. 55
Benson P.J., Myers P.C., 1989, ApJS 71, 89
Bettens R.P., Lee H.H., Herbst E., 1995, ApJ 443, 664
Black J.H., Dalgarno A., 1977, ApJS 34, 405
Bohlin R.C., Savage B.D., Drake J.F., 1978, ApJ 224, 132
Boland W., de Jong T., 1984, A&A 134, 87
Brown P.N., Byrne G.D., Hindmarsh A.C., 1989, SIAM J. Sci. Stat. Comput. 10, 1038
Cardelli J.A., Meyer D.M., Jura M., Savage B.D., 1996, ApJ 467, 334
Charnley S.B., Dyson J.E., Hartquist T.W., Williams D.A., 1988, MNRAS 235, 1257
Chlewicki G., Greenberg J.M., 1984, MNRAS 211, 719
Cox P., Güsten R., Henkel C., 1988, A&A 206, 108
Draine B.T., 1978, ApJS 36, 595
Duley W.W., 1974, A&AS 26, 199
Duley W.W., Williams D.A., 1984, Interstellar Chemistry. Academic Press, London
Epstein I.R., 1990, 1989 Lectures In Complex Systems. Addison-Wesley, California, p. 213
de Jong T., Dalgarno A., Boland W., 1980, A&A 91, 68
Federman S.R., Glassgold A.E., Kwan J., 1979, ApJ 227, 466
Fuller G.A., Myers P.C., 1992, ApJ 384, 523
Fuller G.A., Myers P.C., 1993, ApJ 418, 273
Graedel T.E., Langer W.D., Frerking M.A., 1982, ApJS 48, 321
Gredel R., Lepp S., Dalgarno A., 1987, ApJ 323, L137
Gredel R., Lepp S., Dalgarno A., Herbst E., 1989, ApJ 289
Grevesse N., Noels A., 1993, Origin of the elements. Cambridge Univ. Press, Cambridge, p. 15
Hartquist T.W., Nejad L.A.M., Williams D.A., 1993, Dust and Chemistry in Astronomy. IOP Publishing, Bristol, p. 205
Herbst E., Klemperer W.K., 1973, ApJ 185, 505
Herbst E., Leung C.M., 1986, ApJ 310, 378
Hirahara Y., Suzuki H., Yamamoto S., Kawaguchi K., Kaifu N., 1992, ApJ 394, 539
Hirahara Y., Masuda A., Kawaguchi K., Ohishi M., et al., 1995, PASJ 47, 845
Howe D.A., Taylor S.D., Williams D.A., 1996, MNRAS 279, 143
Iglesias E., 1977, ApJ 218, 697
Irvine W.M., Goldsmith P.F., Hjalmarson Å., 1987, Interstellar Processes. D. Reidel Publishing, p. 561
Lambert D.L., Sheffer Y., Gilliland R.L., Federman S.R., 1994, ApJ 420, 756
Langer W.D., Velusamy T., Kuiper T.B.H., et al., 1995, ApJ 453, 293
Le Bourlot J., Pineau des Forêts G., Roueff E., 1995a, A&A 297, 251
Le Bourlot J., Pineau des Forêts G., Roueff E., 1995b, A&A 302, 870
Lee H.H., Herbst E., Pineau des Forêts G., Roueff E., Le Bourlot J., 1996, A&A 311, 690
Lee H.H., Roueff E., Pineau des Forêts G., et al., 1998, A&A 334, 1047
Léger A., 1983, A&A 123, 271
Léger A., Jura M., Omont A., 1985, A&A 144, 147
Maloney P., 1988, ApJ 334, 761
Matthews H.E., Irvine W.M., 1986, Masers, Molecules, and Mass Outflows in Star Forming Regions. Haystack Observatory, Westford, MA, p. 1
McCutcheon W.H., Dickman R.L., Shuter W.L.H., Roger R.S., 1980, ApJ 237, 9
McLaughlin D.E., Pudritz R.E., 1996, ApJ 469, 194
McLaughlin D.E., Pudritz R.E., 1997, ApJ 476, 750
Meyer D.M., Cardelli J.A., Sofia U.J., 1997, ApJ 490, L103
Meyer D.M., Jura M., Cardelli J.A., 1998, ApJ 493, 222
Millar T.J., Freeman A., 1984, MNRAS 207, 405
Millar T.J., Herbst E., 1990, A&A 231, 466
Millar T.J., Nejad L.A.M., 1985, MNRAS 217, 507
Millar T.J., Farquhar P.R.A., Willacy K., 1997, A&AS 121, 139
Minh Y.C., Irvine W.M., Ohishi M., et al., 1993, A&A 267, 229
Mitchell G.F., Ginsburg J.L., Kuntz P.J., 1978, ApJS 38, 39
Myers P.C., 1990, Molecular Astrophysics – A Volume Honouring Alexander Dalgarno. Cambridge University Press, Cambridge, p. 328
Myers P.C., Fuller G.A., Goodman A.A., Benson P.J., 1991, ApJ 376, 561
Nejad L.A.M., 1986, Ph.D. Thesis, Univ. Manchester
Nejad L.A.M., Williams D.A., Charnley S.B., 1990, MNRAS 246, 183
Nejad L.A.M., Williams D.A., 1992, MNRAS 255, 441
Nejad L.A.M., Hartquist T.W., Williams D.A., 1994, Ap&SS 220, 261
Ohishi M., Kaifu N., 1998, Chemistry and Physics of molecules and grains in space. Faraday Discussion 109, The Royal Society of Chemistry, London, p. 205
Ohishi M., Irvine W.M., Kaifu N., 1992, Astrochemistry of Cosmic Phenomena. Kluwer, Dordrecht, p. 171
Palumbo M.E., Geballe T.R., Tielens A.G.G.M., 1997, ApJ 479, 839
Peng R., Langer W.D., Velusamy T., Kuiper T.B.H., Levin S., 1998, ApJ 497, 842
Pineau des Forêts G., Roueff E., Flower D.R., 1992, MNRAS 258,45
Prasad S.S., Huntress W.T. Jr., 1980, ApJS 43, 1
Prasad S.S., Tarafdar S.P., 1983, ApJ 267, 603
Pratap P., Dickens J.E., Snell R.L., et al., 1997, ApJ 486, 862
Rawlings J.M.C., Hartquist T.W., Menten K.M., Williams D.A., 1992, MNRAS 255, 471
Saito S., Kawaguchi K., Yamamoto S., et al., 1987, ApJ 317, L115
Schilke P., Keene J., Le Bourlot J., Pineau des Forêts G., Roueff E., 1995, A&A 294, L17
Scott S.K., 1994, Oscillations, Waves, and Chaos in Chemical Kinetics. Oxford University Press, Oxford
Shu F.H., Milione V., Gebel W., et al., 1972, ApJ 173, 557
Smith D., Adams N.G., Giles K., Herbst E., 1988, A&A 200, 191
Sternberg A., Dalgarno A., 1995, ApJS 99, 565
Suzuki H., Yamamoto S., Ohishi M., Kaifu N., Ishikawa S., 1992, ApJ 392, 551
Tielens A.G.G.M., Whittet D.C.B., 1997, Molecules in Astrophysics; Probes & Processes. Kluwer, Dordrecht, p. 45
Turner B.E., 1994, ApJ 420, 661
Turner B.E., Lee H.H., Herbst E., 1998, ApJS 115, 91
van Dishoeck E.F., Black J.H., 1986, ApJS 62, 109
van Dishoeck E.F., Black J.H., 1988, ApJ 334, 771
van Dishoeck E.F., 1998, Chemistry and Physics of molecules and grains in space. Faraday Discussion 109, The Royal Society of Chemistry, London, p. 31
Viala Y.P., 1972a, Thesis, Observatoire de Meudon
Viala Y.P., 1972b, Compt. Rend. Acad. Sci. (Paris), 275B, 117
Viala Y.P., Horedt G.P., 1974, A&A 33, 195
Wagenblast R., Hartquist T.W., 1988, MNRAS 230, 363

Wagenblast R., Hartquist T.W., 1989, MNRAS 237, 1019
Whittet D.C.B., 1993, Dust and Chemistry in Astronomy. IOP Publishing, Bristol, p. 9
Whittet D.C.B., Schutte W.A., Tielens A.G.G.M., et al., 1996, A&A 315, L357
Williams D.A., 1993, Dust and Chemistry in Astronomy. IOP Publishing, Bristol, p. 143
Williams D.A., 1998, Chemistry and Physics of molecules and grains in space. Faraday Discussion 109, The Royal Society of Chemistry, London, p. 1
Willacy K., Williams D.A., 1993, MNRAS 260, 635
Willacy K., Williams D.A., Duley W.W., 1994, MNRAS 267, 949
Wolkovitch D., Langer W.D., Goldsmith P.F., Heyer M., 1997, ApJ 477, 241
Xie T., Allen M., Langer W.D., 1995, ApJ 440, 674
Yamamoto S., Saito S., Kawaguchi K., et al., 1987, ApJ 317, L119